

**Evidence for Surface α
Particle Clusters in
nat ^{197}Au from the
(e, α) Reaction**

W. R. Dodge

**U.S. DEPARTMENT OF COMMERCE
National Institute of Standards
and Technology
Physics Laboratory
Gaithersburg, MD 20899**

**U.S. DEPARTMENT OF COMMERCE
Robert A. Mosbacher, Secretary
NATIONAL INSTITUTE OF STANDARDS
AND TECHNOLOGY
John W. Lyons, Director**

NIST



**Evidence for Surface α
Particle Clusters in
nat ^{197}Au from the
(e, α) Reaction**

W. R. Dodge

**U.S. DEPARTMENT OF COMMERCE
National Institute of Standards
and Technology
Physics Laboratory
Gaithersburg, MD 20899**

June 1991



**U.S. DEPARTMENT OF COMMERCE
Robert A. Mosbacher, Secretary
NATIONAL INSTITUTE OF STANDARDS
AND TECHNOLOGY
John W. Lyons, Director**



Evidence for surface α particle clusters in ^{nat}Ag and ^{197}Au
from the (e,α) reaction

W. R. Dodge[†]
8200 Raymond Lane
Potomac, Maryland 20854-3727

The ^{nat}Ag and ^{197}Au (e,p) and (e,α) energy and angular distributions were measured at 6 electron bombarding energies between 50 and 115 MeV at the National Institute of Standards and Technology. The ^{nat}Ag and ^{197}Au (e,p) angular distributions exhibit an asymmetric component which increases from 0 to 50% as the proton energy increases from the proton Coulomb barrier to 26 MeV. The ^{nat}Ag and ^{197}Au (e,α) angular distributions exhibit an asymmetric component which increases from 0 to 30% as the α energy increases from the α particle Coulomb barrier to 26 MeV. We conclude that the asymmetric component of the proton and α particle yields are the result of direct or semidirect processes rather than resonance processes and hence, because of the short mean free paths of α particles in nuclear matter, give evidence for the existence of α particle clusters in the nuclear surface.

[†]The experimental work reported in this paper was carried out while the author was an employee of the National Institute of Standards and Technology.

I. INTRODUCTION

The hypothesis that nucleons in the surface of a heavy nucleus are correlated in α particle clusters of the type hypothesized by Wilkinson¹ has received experimental support from several different sources. These sources are the ratio of the theoretical and experimental values of the reduced widths for α decay in α emitters,¹ knockout reactions produced by protons and alphas, ($\alpha, 2\alpha$) coincidence experiments,² and K meson capture from circular orbits.¹ To these traditionally quoted sources of evidence for surface α particles has recently been added evidence from α transfer reactions such as ($d, {}^6\text{Li}$),³ (n, α) scattering experiments,⁴ ($p, p'\alpha$),⁵ and fast π nuclear scattering.⁶ These experiments have all contributed to the plausibility of the hypothesis of nuclear surface α particles. Of these experiments, the ($\alpha, 2\alpha$) and ($p, p'\alpha$) coincidence experiments are the most convincing, while the fast $N(\pi, \pi')N^*$ inelastic scattering experiments, in which the product nuclei were detected by their radioactivity, can be explained in terms of theories which do not assume α clusters according to Chang et al.⁷

Arguments for the occurrence of α particles in the nuclear surface are based, in part, on the fact that in the nuclear surface the nucleon density is low, and hence the Pauli principle does not inhibit formation of nucleons into α clusters as strongly as it does in the nuclear interior. Brink and Castro have studied the importance of α clustering in the interior regions of heavy nuclei by studying the existence of such phenomena in infinite nuclear matter.⁸ They showed that at normal nucleon densities a uniform nucleon density distribution is more stable than the α cluster nucleon density distribution, indicating that α types of correlations are not important in the interior regions of heavy nuclei. However, at nucleon densities of $\approx .3$ of the central nuclear density of $.068$ nucleons/ fm^3 , a transition occurs and the α cluster distributions becomes more stable than the uniform density distribution, indicating that α clusters should be very important in the surface of a heavy nucleus. While these α particle clusters are of obvious importance in a description of the texture of the nuclear surface and as examples of nuclear correlations, their relevance to theories of photonuclear physics was not clear. Recently, however, Kuo, Blomqvist, and Brown⁹, KKB, have pointed out that the presence of α clusters in the nuclear surface could partially resolve a discrepancy between Brown's microscopic model of the photonuclear effect and experiment in ${}^{208}\text{Pb}$. According to KKB,⁹ these alphas would tend to limit the volume in which protons oscillate against neutrons to the nuclear interior, since protons and neutrons are bound together strongly in the α particle. Furthermore, these alphas could provide a basis for the assumption of the macroscopic hydrodynamic models that the proton and neutron relative velocity is zero at some nuclear radius.⁹

Motivated by these theoretical conjectures about the existence of α clusters in the nuclear surface, we have searched for effects in the (e, α) reaction which could be attributed to these clusters. We measured the (e, p) and (e, α) energy and angular distributions from Be, ^{107}Ag and ^{197}Au at several electron bombarding energies between 50 and 115 MeV. Defining the asymmetry of the measured angular distribution to be $(f-b)/(f+b)$, where f and b are equal to $d\sigma/d\Omega$ integrated from 0 to $\pi/2$ and $\pi/2$ to π , respectively, our ^{107}Ag and ^{197}Au $d\sigma(e, p)/d\Omega$ exhibit an asymmetry which increases from ≈ 0 to 50% as the proton energy increases from the Coulomb barrier to 25 MeV. In contrast, our $d\sigma(e, \alpha)/d\Omega$ have an asymmetry which increases from ≈ 0 to 30% as the α energy increases from the Coulomb barrier to 25 MeV. Below the Coulomb barrier, our $d\sigma(e, \alpha)/d\Omega$ are backward peaked. Reactions which exhibit angular distribution asymmetries as a function of the particle kinetic energy are typical of direct reactions.¹⁰ Therefore, we conclude that the asymmetry of our $d\sigma(e, \alpha)/d\Omega$ must be attributed to a direct or semidirect process involving alphas which are not formed by slow statistical processes during de-excitation of the nucleus.

II. EXPERIMENTAL PROCEDURE

The National Institute of Standards and Technology's (formerly the National Bureau of Standards) linear electron accelerator, linac, provided a spatially resolved and momentum analyzed beam of electrons which was incident on self-supporting ^{107}Ag , ^{197}Au , and Be targets. The ^{107}Ag , ^{197}Au , and Be target mass thicknesses were 3.10, 5.23, and 14.95 mg/cm², respectively. A magnetic spectrometer¹¹ was used to provide particle momentum/charge analysis and five Si surface barrier detectors of thicknesses varying from 150 to 400 μm and positioned in the spectrometer focal plane provided either particle energy or energy loss which was used in particle identification. In addition, three of the focal plane detectors, FPDs, were backed up by 500 μm surface barrier detectors. Above ≈ 3.25 MeV, protons were transmitted through the FPDs. Hence, the proton energy loss peak in the FPDs was displaced from the total absorption position to a position below the triton peak, τ , for most of the proton energies measured in this experiment. Between ≈ 3.25 and 8.2 MeV protons and alphas could be simultaneously detected in both the focal plane and backing detectors. At energies above 8.2 MeV, protons and alphas could not be simultaneously detected in the focal plane detectors because of the finite pulse-height acceptance of the data logging analogue-to-digital converters, ADCs, and hence above 8.2 MeV, protons were only counted in the backing detectors. The relative detection efficiencies of the focal plane and backing detectors above 8.2 MeV were compared and found to be $.96 \pm .01$, $.95 \pm .01$ and $.97 \pm .01$.

The momentum acceptance interval, Δp , of each detector was determined with ^{210}Po and ^{148}Gd α sources (α energies of 5.304 and

3.18 MeV). The momentum acceptance interval was corrected for the fact that the focal plane detectors were round and the electron beam spot width projected on the target was not equal to the α source width. This correction, $\mathcal{C}(W_s, W_B)$, to Δp was

$$\mathcal{C}(W_s, W_B) = \frac{W_B \left[\sin^{-1} W_{SD} + W_{SD} \sqrt{1 - W_{SD}^2} \right]}{W_s \left[\sin^{-1} W_{BD} + W_{BD} \sqrt{1 - W_{BD}^2} \right]}, \quad (1)$$

where W_s and W_B are the width of the α source and electron beam, respectively, and W_{SD} and W_{BD} are the ratios of these quantities to the focal plane detector diameter times the magnet magnification. This correction to Δp was never larger than 6%. Data from each were normalized relative to the central FPD by comparing the energy spectra of each detector in energy intervals .92 MeV wide where the spectra overlapped.

A typical pulse height spectrum produced by the charged disintegration products of Be is shown in Fig. 1. The energy of the alphas and protons is 4.5 MeV. The continuous background shown between the prominent peaks produced by the charged particle disintegration products shown in Fig. 1 had two components: (1) a contribution from momentum analyzed particles produced in the target ladder, (2) a continuous contribution from electron, photon, and neutron induced events not momentum analyzed and not produced in the target or target ladder. Background from (1) was measured with the target ladder retracted and was found to be negligible. Information about background (2) was provided in regions of the pulse height spectra in regions between well resolved mass groups. Background component (2) was only important for the highest energy protons where the energy deposited in the rear detector became < 1 MeV. In these cases, background (2) was subtracted from the pulse height spectra by a non-linear least squares fitting program. The counts extracted from the various mass groups in the FPD pulse height distributions after (2) were subtracted were divided by the number of incident electrons, e , by the mean energy of the energy acceptance interval, $2\Delta p/p$, of the detector appropriate to the particle charge state and mass to correct for the spectrometer magnet dispersion.

The data were corrected for energy loss in the target using energy loss data compiled by Janni.¹² The mean target thickness assumed in the energy loss calculations was half the actual target thickness divided by the cosine of the angle between the plane of the target foil and the spectrometer magnet symmetry axis. The α energy loss in the ^{107}Ag , ^{197}Au , and Be targets never exceeded .15, .16, and 1.5 MeV, respectively.

The other components of the apparatus used in the experiment (i.e., the linac and electron beam momentum analyzing and handling system) have been described previously.¹¹ The incident electron

beam momentum transmission interval, $(\Delta p/p)_c$, was $\pm 1\%$. The incident electron beam current was measured with two ferrite toroid induction current monitors. Beam current measurements made with these monitors deviated from each other by $< 1.5\%$ during the experiment. The ferrite monitors were calibrated against a standard water cooled NIST beam dump. The calibration constant did not depend on energy between 20 and 110 MeV. Typically, all data at a given angle were taken in a 12 hour period.

Energy spectra were obtained for ^{109}Ag , ^{197}Au , and Be as a function of the angle, $\theta_{\alpha \text{ or } p}$, between the incident electron beam and the detected particle, and as a function of the bombarding electron energy E_0 . Data for ^{109}Ag and ^{197}Au were taken at $\theta_{\alpha \text{ or } p} = 34^\circ, 48^\circ, 62^\circ, 90^\circ$, and 146° with $E_0 = 50$ and 110 MeV. In addition, data for ^{109}Ag and ^{197}Au at 34° were obtained for $E_0 = 80$ and 110 MeV, and at 90° for $E_0 = 75$ MeV and 100 MeV. Data for Be at 34° were obtained at $E_0 = 50, 80, 100,$ and 110 MeV and at 90° at $50, 75, 100$ and 110 MeV.

III. RESULTS

The proton and alpha yields/MeV/target nuclei/sr/e at the various angles for a given value of E_0 were least squares fitted to an expansion in Legendre polynomials. The coefficients of the angular distribution expressed in the center of mass system, *cms*, are given by

$$A_\ell^{\text{cms}} = A_\ell + \Gamma \ell(\ell+1) \left[\frac{A_{\ell+1}}{(2\ell+3)} - \frac{A_{\ell-1}}{(2\ell-1)} \right], \quad (2)$$

$$\text{with } \Gamma = \frac{q}{M_t} \sqrt{\frac{M_p}{2T_p}} < 1.$$

In this expression q is the virtual photon momentum transfer, M_p and M_t are the particle and target mass numbers, and T_p is the particle kinetic energy. The momentum transfer, q , is not measured in this experiment, but for Ag and Au the maximum possible momentum transfer, $2E_0/c$, results in a difference between most angular distribution coefficients expressed in the laboratory or *cms* within errors of the coefficients. The coefficient A_0 is shown in Fig. 2 and the ratios of coefficients A_1/A_0 , A_2/A_0 , and A_3/A_0 are shown in Figs. 3 through 13 for ^{109}Ag and ^{197}Au . The curve for A_0 multiplied by 4π represents the energy spectrum integrated over particle emission angles. The uncertainties in the input data have contributions from counting statistics and from the effective target thickness. The uncertainties in the effective target thickness are generated by electron beam heating changes in the angle between the incident beam and the target foil. In cases where the angle between the normal to the plane of the target foil

and the incident electron beam was small, the uncertainty in the effective target thickness was the dominant uncertainty. The ratio of the coefficients A_1/A_0 and A_3/A_0 were least squares fitted to an expression of the form $a_0+a_1T_p$ over certain energy intervals with statistically significant χ . The angular distribution asymmetries (defined in the INTRODUCTION) derived from these fits together with the average asymmetries computed in the given range of T_p and computed in an energy interval 10 MeV wide, starting where the asymmetries become positive, are given in Table I. Fig. 14 shows the differential energy spectrum of the Be(e, α) reaction at 34° for $E_0 = 50$ and 110 MeV.

The salient features of the energy and angular distributions are: (1) the ^{nat}Ag and $^{197}\text{Au}(e,\alpha)$ angular distribution asymmetries increase by $\approx 30\%$ as E_0 is increased from 50 to 110 MeV, (2) the ^{nat}Ag and $^{197}\text{Au}(e,p)$ angular distribution asymmetries increase by $\approx 50\%$ as E_0 is increased from 50 to 110 MeV, and (3) the $^{197}\text{Au}(e,\alpha)$ total energy distribution peak moves to a slightly lower energy as E_0 increases from 50 to 110 MeV. In contrast, the $^{nat}\text{Ag}(e,\alpha)$ and (e,p) and the $^{197}\text{Au}(e,p)$ energy distribution peaks remain fixed in energy as E_0 changes from 50 to 110 MeV.

The ^{nat}Ag and ^{197}Au proton and alpha yields/MeV/target nuclei/sr/e as a function of the incident electron energy, E_0 at 34° and 90° are shown in Figs. 15 through 18. The data were averaged over somewhat larger particle energy intervals than were data presented in the angular distributions in the interest of compactness. The excitation data shown in Figs. 15 through 18 can be converted into differential cross sections by the virtual photon difference unfolding method,

$$\left[\left\langle \frac{d\sigma(k, \theta)}{d\Omega} \right\rangle \right]_{\theta} = \frac{[Y(E_{0_2})]_{\theta} - [Y(E_{0_1})]_{\theta}}{\int_{thres}^{E_{0_2}} \frac{N(E_{0_2}, k)}{k} dk - \int_{thres}^{E_{0_1}} \frac{N(E_{0_1}, k)}{k} dk} \quad (3)$$

where $[Y(E_{0_1})]_{\theta}$ is the yield/MeV/target nuclei/target nuclei/sr/e at an angle of θ and $N(E_{0_1})$ is given by

$$N(E_0, k) = \frac{\alpha}{\pi} \left[1 + \left(\frac{E_0 - k}{E_0} \right)^2 \right] \left\{ \ln \left[\frac{2E_0(E_0 - k)}{m_e k} \right] - \frac{2(E_0 - k)}{E_0} \right\} \quad (4)$$

Cross sections for $^{197}\text{Au}(e,p)$ and (e,α) derived with these assumptions are shown in Fig. 19. Although the uncertainties are large and the points few, a significant difference is seen between the trend of the (e,p) and the (e,α) $d\sigma/d\Omega$. The same remarks apply to the $^{nat}\text{Ag}(e,p)$ and (e,α) $d\sigma/d\Omega$ shown in Fig. 20.

IV. DISCUSSION

The primary motivation for this experiment was to search for anomalies in the yields of α particles from Ag and Au at electron bombarding energies above 50 MeV which might be related to α clusters in the nuclear surface. Since Be is known to exhibit considerable α clustering, the Be(e, α) yields were intended to provide a reference frame with which to compare our ^{107}Ag and ^{197}Au (e, α) yields. By anomalies we mean features of the (e, α) energy and angular distributions which can not be explained in terms of pre-equilibrium (precompound) or equilibrium statistical models. The (e, α) yields could be due to: (1) quasi-free electron scattering from literal α clusters with the ejection of recoil α cluster from the nucleus; (2) absorption of a virtual photon by the usual photonuclear photon absorption mechanisms, including photon absorption by a quasideuteron, followed by precompound and eventually compound nucleus formation and evaporation of an alpha; (3) photon absorption by a quasideuteron with the fast (p,n) pair interacting with the remaining nucleons via the same or similar interactions responsible for (p, α) and (n, α) scattering; (4) direct interaction of a virtual photon with an α cluster and the remainder of the nucleus in the sense of the direct photodisintegration models. This list is not exclusive but includes mechanisms we believe most likely to be responsible for the observed α yields. **Items 2, 3 and 4** involve conventional photonuclear processes. Assuming the existence of α clusters, it is probable that all of the above **items** would contribute to our (e, α) yields. If a certain fraction of our α yields result from direct processes, such as outlined in **items 1, 3, and 4**, the existence of "surface" α clusters, because of the short mean free paths of alphas in the nuclear interior, is established. On the other hand, the compound nuclear or statistical models of **item 2** have no predictive powers concerning the origin or existence of α clusters since all dynamical aspects of the evaporation process are implicitly contained in the reaction or inverse cross section data which are an input into the calculation.

We now consider the possibility that a significant fraction of our α yields are produced by the mechanism of **item 1**, namely, quasifree scattering. Because of the kinematic incompleteness of an (e, α) experiment (i.e., the scattered electron and the α were not detected in coincidence), these data can only indicate the plausibility of such a process, but cannot unambiguously indicate its existence. However, our (e, α) and (e,p) measurements, together with an α particle energy loss in the target comparable to the proton energy loss in an (e,e'p) experiment, indicate that the (e,e' α) counting rate in a heavy nucleus should be $\approx .05\%$ of the (e,e'p) counting rate. Hence, (e,e' α) coincidence experiments are still far in the future even at laboratories with electron linacs with 100% duty factors. Furthermore, few, if any (e, α) experiments have been reported.

Here we estimate the magnitude of the quasifree α scattering component. If this component were produced by elastic scattering on ${}^4\text{He}$, then the angular distribution of these alphas in the laboratory system would be given by the Mott scattering cross section

$$\left[\frac{d\sigma}{d\Omega} \right]_{\text{Mott}} = \left(\frac{2e^2}{E_0} \right)^2 \frac{\sin^2\theta_\alpha}{\cos^3\theta_\alpha} \frac{(1+\rho)^4}{1+2\rho+\rho^2\sin^2\theta_\alpha} \mathcal{F}^2(q^2), \quad (5)$$

where θ_α is the angle between the elastically scattered α and the incident electron of total energy E_0 , $\rho = E_0/M_\alpha$, M_α is the α particle mass, $\mathcal{F}(q^2)$ is the elastic scattering form factor of ${}^4\text{He}$. If a real nucleus has " α clusters", this angular distribution will be modified by the momentum distribution of these alphas, by scattering of these alphas by other nucleons in the nuclear surface, by the Coulomb barrier, and by the number of " α particles" with mean-free paths such that these alphas escape from the nucleus.

An estimate of the total cross section for recoil α -production from a ${}^4\text{He}$ target with α energies above a cutoff energy, T_{\min} , can be obtained by integration of the Mott cross section, neglecting final state interactions (assuming only the Coulomb interaction is important) and assuming

$$\mathcal{F}^2(q^2) = e^{-\langle r^2 \rangle q^2/3}, \quad (6)$$

which is a good approximation for $q^2 < 6\text{fm}^{-2}$.¹³ Here \mathbf{q} is the usual 3-vector momentum transfer. The total elastic electron scattering cross section on ${}^4\text{He}$,

$$\begin{aligned} \sigma_{T_{\text{Mott}}} = \pi \left(\frac{2e^2}{E_0} \right)^2 & \left\{ \frac{(1+\rho)^2(1-x^2)}{x^2} + \left[(1+2\rho) - \frac{4}{3}E_0^2\langle r^2 \rangle \right] \ln \left[\frac{(1+2\rho)x^2}{(1+\rho)^2 - \rho^2x^2} \right] \right. \\ & - \frac{4}{3}E_0^2\langle r^2 \rangle \frac{1-x^2}{(1+\rho)^2 - \rho^2x^2} \\ & \left. + \frac{2}{9}E_0^4\langle r^2 \rangle^2 \left[\frac{1}{(1+\rho)^2 - \rho^2x^2} - \frac{1}{[(1+\rho)^2 - \rho^2x^2]^2} \right] \right\}, \end{aligned} \quad (7)$$

where

$$x^2 = \cos^2\theta_{\max} = \frac{T_{\min}(1+\rho)^2}{\rho^2(T_{\min} + 2M_\alpha)}. \quad (8)$$

The total number of recoil alphas from elastic electron scattering on ${}^4\text{He}$ as a function of E_0 is shown in Fig. 21 for various values of T_{\min} . The number of α particles to be associated with quasifree scattering depends on the minimum kinetic energy which an α must have for the probability for penetration through the Coulomb barrier to be ≈ 1 . Brink and Castro's⁸ infinite nuclear matter calculation indicated that the Fermi momentum at nucleon densities where α clustering becomes important is about 200 MeV/c ($k_F \approx 1 \text{ fm}^{-1}$) corresponding to α kinetic energies of 5 MeV. On the other hand, Dubost et al¹⁴ assumed an average kinetic energy of 10 MeV for α particles in the nuclear surface in analyzing their (p, α) data. Igo,² following Rasmussen,¹⁵ on the basis of an optical model analysis of (α, α') data, conjectured that α particles might have a stable existence where the nuclear density is $\approx 5\%$ of the central nucleon density. For ${}^{197}\text{Au}$ this corresponds to a radius of 8 fm and a Coulomb barrier energy, T_C , of 14 MeV. In order to obtain an estimate of the number of quasifree (e, α) events we would observe if N_α α particles existed in a real nucleus, we use the momentum distribution of the oscillator well¹⁶

$$\rho_\alpha(p) = \left[1 + \frac{4}{3} \left(\frac{p}{p_0} \right)^2 \right] e^{-\left(\frac{p}{p_0} \right)^2}. \quad (9)$$

The oscillator well parameter $p_0 = 198.7(Z/A)^{1/3}$ MeV. The momentum distribution of a nucleon in the oscillator well after scattering is given by $\rho_\alpha(\mathbf{P})$, where $\mathbf{P}^2 = \mathbf{p}^2 + \mathbf{q}^2 - 2\mathbf{p} \cdot \mathbf{q}$. This momentum distribution is to be integrated over all orientations and magnitudes of \mathbf{p} compatible with $p \geq p_C = \sqrt{M_\alpha T_C}$. The number of quasifreely scattered particles, N_α , with energies above the Coulomb barrier T_C is

$$N_\alpha = 2\pi N_\alpha^0 \int_0^{\theta_{\max}} \sigma_{\text{Mott}} \mathcal{F}^2(\mathbf{q}^2) \mathcal{R}_\alpha(\mathbf{q}^2) d(\cos\theta_\alpha), \quad (10)$$

where

$$\mathcal{R}_\alpha(q) = \frac{\iint \rho_\alpha(P) p^2 dp d\Omega_{pq}}{p \geq q} \quad (11)$$

is the fraction of recoil particles with momenta $P \geq p_C$. The expression $\mathcal{R}_\alpha(q)$ for the oscillator well is derived in Appendix I.

While a Fermi gas model is not appropriate for an α particle gas, we have also computed $\mathcal{R}_F(q)$ for a Fermi gas momentum distribution in the limit of infinite dilution.

In this case,

$$\mathfrak{R}_F(q) = \frac{1}{2} - \frac{1}{2} \left(\frac{p_C}{k_F} \right)^3 - \frac{1}{4} \left(\frac{q}{k_F} \right)^3 + \frac{3}{4} \left(\frac{q}{k_F} \right) + \frac{3}{16} \left(\frac{k_F}{q} \right) \left[\left(\frac{p_C}{k_F} \right)^2 + \left(\frac{q}{k_F} \right)^2 - 1 \right]^2$$

for $k_F + q \geq p_C \geq q$, (12)

$$\mathfrak{R}_F(q) = \left[\frac{3}{4} \left(\frac{q}{k_F} \right) - \frac{1}{16} \left(\frac{q}{k_F} \right)^3 \right] \text{ for } k_F = p_C > q.$$

Note that the expression for $R_F = p_C > q$ is the response function given by deForest and Walecka¹⁷ for quasifree (e,p) scattering. The Fermi momentum k_F was taken to be $315(Z/A)^{1/3}$ MeV. For ¹⁹⁷Au with $\theta_{\max} = 66.1^\circ$, corresponding to a minimum α recoil energy of 1 MeV at $E_0 = 110$ MeV, Eq. (10) predicts $.8 \times 10^{-30} N_\alpha$ for an oscillator momentum distribution with $p_0 = 147$ MeV/c, $p_C = 376$ MeV/c, and $.4 \times 10^{-30} N_\alpha$ for a Fermi momentum distribution with $k_F = 232$ MeV/c. For ^{nat}Ag, the corresponding estimates are $.30 \times 10^{-29} N_\alpha$ and $.25 \times 10^{-29} N_\alpha$ with $p_C = 318$ MeV/c. Increasing p_0 and k_F by a factor of 1.5 increases the ¹⁹⁷Au estimates to $.6 \times 10^{-29} N_\alpha$ and $.9 \times 10^{-29} N_\alpha$, while changing T_{\min} to 3 MeV decreases the Au estimate by a factor of 10.5. Thus estimates obtained from Eq. (10) are subject to large uncertainties because of their sensitivity to changes in T_{\min} and p_0 , and also because the impulse approximation may not be valid at these electron energies. Of course, only the asymmetric component of our ^{nat}Ag(e, α) and ¹⁹⁷Au(e, α) energy spectra, integrated over α energies and angles, can be attributed to quasifree scattering. At $E_0 = 110$ MeV, these are 13 and 14%, respectively, of the total yields. Taking into account theoretical uncertainties, and using $p_0 = 185$ MeV/c and $T_{\min} = 2$ MeV, our data for $E_0 = 110$ MeV are compatible with $2.3 \pm_{2.1}^5$ and $.5 \pm_{.4}^5$ alphas in the nuclear surface of Ag and Au, respectively. Correction for final state interactions would increase these numbers significantly.

Recoil protons from quasifree electron scattering should also contribute to our ^{nat}Ag and ¹⁹⁷Au 110 MeV proton energy spectra. Figure 22 shows the total number of protons elastically scattered above a cutoff energy T_{\min} as a function of E_0 , as predicted by Eq. (10) appropriately modified. Since the proton recoil energy is four times as large as the α recoil energy, and the Coulomb barrier is half as large, recoil protons should be clearly discernible. Information on the proton momentum distribution from (e,e') and (e,e'p) already exists for ¹²C. Inelastic (e,e') data¹⁶ show the width of the ¹²C quasifree elastic scattering peak is ≈ 32 MeV for $E_0 = 98$ MeV and $\theta_c = 135^\circ$. Hence, the width of the quasifree recoil proton energy distribution for $E_0 = 110$ MeV will have a contribution from the Fermi momentum distribution of $q\Delta q/M_p \approx 6$ MeV and will be centered at $E_p = 18$ MeV for $\theta_p = 34^\circ$. However, unlike

alphas in ^{197}Au , which are unbound, the ^{197}Au proton separation energy is 5.8 MeV. The total number of recoil protons above the Coulomb barrier, which is ≈ 9.4 MeV, plus the proton separation energy is $.7 \times 10^{-28}$ protons/Au/e using \mathfrak{R}_F of Eq. (11) with $p_C = 15.2$ MeV. The $^{197}\text{Au}(e,p)$ data shown in Fig. 5 have only a slight inflection at 18 MeV which contains a small fraction, $<20\%$, of the total proton yield of 1.4×10^{-28} protons/Au/e. Moreover, this inflection is also seen in the 50 MeV ^{197}Au data at the same proton energy and is not seen in the $^{nat}\text{Ag}(e,p)$ data shown in Fig. 11. Furthermore, both our ^{nat}Ag and ^{197}Au (e,p) yields fit virtual photon isochromats derived using the assumption that only the proton, scattered electron, and a nucleus in the ground state are in the final state to within 20%. Hence, while proton shell binding energies and other data needed for a proper impulse approximation calculation are not well known for electron energies of 110 MeV, corresponding to reduced electron wavelengths of 1.8 fm, and while the impulse approximation is certainly better for (e,p) than for (e, α) reactions, our failure to observe a measurable quasifree peak in our proton yields leads us to discount quasifree scattering as a viable mechanism with which to explain our (e, α) yields.

We now consider the characteristics of the (e, α) energy and angular distributions which would be produced by the mechanisms suggested in item 2 listed at the beginning of this section. The photonuclear version¹⁸ of the statistical model predicts that the α yields, Y_α , are given by

$$Y_\alpha \propto \int_{thres}^{E_0} \sigma_{\gamma_{abs}}(k) \frac{\Gamma_\alpha(k)}{\sum \Gamma_i(k)} \frac{N(E_0, k)}{k} dk \quad (13)$$

The sum over the partial widths $\Gamma_i(k)$ is over all open decay channels. Here, $\sigma_{abs}(k)$ is the total photon absorption cross section at a photon energy k , $N(E_0, k)$ is defined by Eq. (4), and

$$\Gamma_i(k) \propto \int_{thres}^{T_{max}} \sigma_{R_i}(T) T \rho(k - S_i - \Delta - T) dT \quad (14)$$

In Eq. (14) $\sigma_{R_i}(T)$ is the reaction cross section for the i th particle of mass number A_i on a nucleus of mass number $(A - A_i)$, and ρ is the density of states in the daughter or residual nucleus. In the Fermi gas model,

$$\rho(k - S_i - \Delta - T) = e^{2\sqrt{a(k - S_i - \Delta - T)}} \quad (15)$$

where a is the level density parameter and is generally taken to be a function of the charge and mass of the residual nucleus,¹⁹ S_i is the separation energy for the i th particle, and T_{max} is defined by $E_0 - S_i - \Delta - T_{max} = 0$. The pairing energy, Δ , is $22/\sqrt{A}$ for an even-odd and

$44/\sqrt{A}$ for an even-even nucleus.

The cross section/MeV, $d\sigma_\alpha/dT_\alpha$, is given by

$$\left(\frac{d\sigma}{dT}\right)_\alpha \propto \int_{thres}^{E_0} \sigma_{abs}(k) \frac{\sigma_{R_\alpha} T_\alpha \rho(k - S_\alpha - \Delta - T_\alpha) N(E_0, k)}{\sum \Gamma_i(k)} \frac{1}{k} dk \quad (16)$$

Figs. 23 and 24 show the $d\sigma/dT_\alpha$ obtained from Eq. (16) for ^{197}Au (e,p) and (e, α) reactions using the values of a , Δ , and σ_R suggested by Dostrovsky et al.¹⁹ The photon absorption cross section was approximated by a Lorentz function which fit the $^{197}\text{Au}(\gamma,n)$ data in the energy regime of the giant dipole resonance and by the quasideuteron model of Levinger²¹ with the Levinger parameter, \mathcal{L} , equal to 10.6. The quenching factor, which determines how fast the giant resonance cross section is turned off and how fast the quasideuteron cross section is turned on, was $1 - e^{-(k-40)/10}$. Decreasing the level density parameter, a , from 14.9/MeV to 10/MeV increases the cross section by ≈ 20 . Obviously a value of the level density parameter between these values would fit the $^{197}\text{Au}(e,p)$ data. However, the same set of parameters grossly overestimates the $^{197}\text{Au}(e,p)$ cross section. The poor quality of the fits reflects the general inadequacy of this simple version of the statistical model. Good fits to (γ,α) energy spectra obtained at lower photon endpoint energies²² are the result of renormalization of the cross section magnitudes or use of unrealistic level density parameters, a , coupled with the cutoff of the bremsstrahlung photon spectrum. Within the framework of this model, the $d^2/d\Omega_\alpha/dT_\alpha$ are isotropic, although Ericson and Strutinski²³ modified the model so that angular distributions symmetric about 90° can be obtained. In general, this model¹⁸ predicts a differential cross section $d^2\sigma(e,\alpha)/d\Omega_\alpha dT_\alpha$ which reaches a maximum a few MeV above threshold of the reaction cross section Coulomb barrier and then decreases rapidly.

Gabriel and Alsmiller,²⁴ GA, have modified the conventional statistical model by incorporating an intranuclear cascade model and photon absorption by the quasideuteron mechanism²¹ to provide both a mechanism for increasing the cross section at photon energies above the giant resonance and for introducing a forward asymmetry in the emitted neutron and proton angular distributions. A still more sophisticated version of GA's calculation which includes photon absorption by π photoproduction on single nucleons has been used by Adler et al.²⁵ to interpret the yield of alphas produced by 500 MeV bremsstrahlung on ^{197}Au . The GA calculation, modified by Adler et al.²⁵ to include the effects of Coulomb barrier penetration, predicts an isotropic α angular distribution which is entirely isotropic in the center of mass system. This isotropic angular distribution transforms to the laboratory system to $d\sigma/d\Omega_{lab} \approx a_0 P_0(\cos\theta) + a_1 P_1(\cos\theta)$, where $a_1/a_0 \approx .054 \approx 2v_{cms}/v_\alpha$. However, the angular distributions of Adler et al.²⁵ exhibited a forward peaked anisotropic component of 16% of the total yield which lead them to

conclude this fraction of their yield resulted from direct processes.

The $d\sigma/dT$ /unit energy loss by radiation, ϕ_{Rad} , where

$$\phi_{Rad} = \int_0^{E_0} \frac{N(E_0, k)}{E_0} dk, \quad (17)$$

is referred to as the differential cross section/equivalent quantum by Adler et al²⁵. If we convert our data to a similar quantity using for $N(E_0, k)$ the virtual photon spectrum defined in Eq. (4), we obtain for Au $\approx .51$ mb/eq. quantum at $E_0 = 110$ MeV at the peak of the energy spectrum which can be compared to 2.2 mb/eq. quantum obtained by Adler et al²⁵. The differential cross sections/eq. quantum obtained by Adler et al²⁵ and by this work are shown in Fig. 25. The experimental and theoretical curves of Adler et al²⁵ have been renormalized to agree with our peak cross section. According to the latter's calculation of the energy distribution of photons leading to the emission of at least one α , our α yield/eq. quantum at $E_0 = 110$ MeV should be about 8% of their yield/eq. quantum at 500 MeV. A linear extrapolation of our excitation data, shown in Figs. 14 through 17 to $E_0 = 500$ MeV should be $\approx 18\%$. The differences between our linear extrapolation and the calculation of Adler et al²⁵ can be understood in terms of the energy distribution of photons leading to the emission of at least one α which has a dramatic increase (due to the Δ resonance) above the photopion threshold.

Several pre-equilibrium or precompound statistical models²⁷ have been developed which aspire to provide a unified description of the statistical properties of an excited nucleus at all times after an exciting event, including time intervals short compared to those envisaged in the statistical models^{18,24,25} discussed above. In these models the states of the system are described in terms of the number of particles and holes they contain and state densities are usually evaluated assuming equally spaced single particle states. Complex particles are fabricated by two-body single nucleon pickup processes. Early versions of this model by Cline,²⁸ which treated complex particle emission in the framework of Griffin and Blann,²⁷ ignored the Pauli principle, shell structure, and angular momentum. Later calculations by Běták et al²⁹ can predict the relative integrated energy spectra of p, d, t, and α in α scattering experiments³⁰ to well within an order of magnitude, thus establishing its superiority over evaporation statistical models for describing the gross features of proton and α particle induced complex particle energy spectra.

Neglect of angular momentum by pre-equilibrium models has restricted the predictive powers of this model to the isotropic component of complex particle yields. We speculate here on

difficulties the pre-equilibrium models may have after angular momentum is considered. Whatever mechanism is responsible for our (e,p) yields, at least three more two-body single nucleon pickup processes are necessary to produce an (e, α) event. While single nucleon pickup processes are forward peaked, in general, after three consecutive such interactions needed to fabricate an α particle, the emitted α particle angular distribution would be less forward peaked than the angular distribution of the particle which initiated the cascade. However, our (e,p) and (e, α) angular distributions are both forward peaked and not significantly dissimilar. The same remarks apply to (α ,p) and (α , α) angular distributions at an incident α energy of 58 MeV³⁰. These facts imply that the hypothesis of sequential two-body interactions will have to be augmented to satisfactorily account for the experimental data. Of course, even with the inclusion of angular momentum, asymmetric angular distributions will not be predicted by statistical models because of the basic statistical model assumption of random phase relations between matrix elements.

Moreover, the asymmetry does not seem to have a trivial kinematic origin, since transformation of an isotropic angular distribution to the laboratory system fails by an order of magnitude to provide the asymmetry observed in the laboratory for both the (α ,p), (α , α) and our (e,p), (e, α) experiments. Indeed, if we assume that our angular distributions can be explained by a pre-equilibrium statistical model with a few of the nucleons in the nucleus participating in the reaction (a typical situation shortly after the initial interaction) then the maximum number of nucleons which could be in statistical equilibrium when this ensemble emitted an α can be estimated by equating $2(v_{\text{cms}}/v_{\text{lab}}) = (8/N^*)(q/P_{\alpha})$ to our observed α asymmetries, where N^* is the number of nucleons in the ensemble, and q is the momentum transfer of the virtual photon which initiated the reaction. From our ^{nat}Ag and ¹⁹⁷Au (e, α) mean asymmetries in the energy interval between the Coulomb barrier and 25 MeV (.16 and .15, respectively) we estimate $N^* \leq 18$.

The intranuclear cascade model, INC, of Bertini et al³¹ can roughly account for both the inelastic proton energy and angular distributions of 29 and 62 MeV proton-induced reactions³². Like the pre-equilibrium statistical model, the basic assumption of the INC is that the reaction can be represented by a sequence of two-body interactions. Unlike the pre-equilibrium model, the INC is a microscopic model and the trajectory of a given particle is followed through the nucleus by means of the "correct" free particle scattering cross sections. Bertini et al³¹ found that the fit to the inelastic (p,p') data of Bertrand and Peele³² could be improved if their calculation included four particle clusters such as α clusters.

We now explore a model to explain our (e, α) data in which the virtual photon is absorbed by a quasideuteron. In this model, the

fast (p,n) pair which results from photodisintegration of the quasideuteron then interacts with the remaining nucleons in the nucleus as in the (p, α) and (n, α) reactions. This model is suggested by the general trends of the (e, α) cross sections shown in Figs. 19 and 20 which are consistent with the absorption of a virtual photon of mean energy between 80 and 110 MeV. It is also suggested by the similarity of the ratio of the (p, α) to (p,p') inelastic proton scattering cross sections integrated over the same particle energy interval. These ratios derived from Bertrand and Peele's³², BP, (p, α) and (p,p') data for incident proton energies of 29 and 62 MeV are $\approx .1$ and $.9$ for Ag, and $.05$ and $.09$ for Au. Since quasideuteron photon absorption at $E_0 = 110$ MeV would result in fast neutrons and protons with energies \approx between 20 and 50 MeV, we should compare the average of the ratios obtained from (p, α) and (p,p') at 29 and 62 MeV of $.15$ for Ag and $.07$ for Au to our data. Our ratios are $.15$ for Ag and $.045$ for Au at $E_0 = 110$ MeV.

This phenomenological model would also predict that the (e, α) angular distributions would be approximated by folding the (e,p) and (p, α) angular distributions. Hence,

$$\begin{aligned} \left(\frac{d\sigma}{d\Omega}\right)_\alpha &\propto \left(\frac{1}{4\pi A_0^{ep}}\right) \int \sum_l \sum_{l'} A_l^{ep} A_{l'}^{p\alpha} P_l(\cos\theta_{ep}) P_{l'}(\cos\theta_{p\alpha}) d\Omega_p \\ &\propto \left(\frac{1}{4\pi A_0^{ep}}\right) \sum_l A_l^{ep} A_l^{p\alpha} P_l(\cos\theta_{p\alpha}) / (2l+1) \end{aligned} \quad (18)$$

where A_l^{ep} , and $A_l^{p\alpha}$, are the coefficients of an expansion of the (e,p) and (p, α) angular distributions in Legendre polynomials. Bertrand and Peele's³² (p, α) and our (e,p) angular distribution data averaged over $20 \leq T_p \leq 25$ MeV, results in $d\sigma/d\Omega_{\alpha} \propto P_0 + .45P_1 + .03P_2 + .01P_3$ for $T_p = 29$ MeV and $d\sigma/d\Omega_{\alpha} \propto P_0 + .32P_1 - .001P_2 + .01P_3$ for $T_p = 62$ MeV. Our measured $d\sigma/d\Omega_{\alpha} \propto P_0 + .41P_1 - .24P_2 + .01P_3$. If we use the ¹⁹⁷Au(p, α) angular distribution data of Lefort et al³³ at a bombarding proton energy, T_p , of 157 MeV, then Eq. (9) predicts $d\sigma/d\Omega_{\alpha} \propto nP_0 + .14P_1 - .01P_2 + .01P_3$, which does not agree nearly as well with our ¹⁹⁷Au $d\sigma/d\Omega_{\alpha}$ as does the average of the $T_p = 29$ and 62 MeV data of BP.

Lastly, we consider the possibility that a certain fraction of our yields might arise from direct interaction between an α cluster and a virtual photon in the sense of the direct photodisintegration models developed by Courant³⁴ and others³⁵. Such models have been useful in understanding portions of (γ ,p) and (γ ,n) cross sections and angular distributions above the giant resonance in light nuclei. Since we only detected alphas with energies ≤ 26 MeV, this model might be expected to apply to the asymmetric ($\propto \sin^2\theta \cos\theta$) component of our $d\sigma/d\Omega$ which are produced by the absorption of virtual photons with energies < 50 MeV. At higher excitation

energies a large fraction of the virtual photon energy would be retained by the residual nucleus, which is not compatible with the assumptions of this model.

If a certain fraction of our asymmetric alpha and proton yields could be associated with a direct photodisintegration process, say by the existence of a precise correlation between particle kinetic energy, virtual photon excitation energy, and the excitation of relatively simple configurations in the residual nucleus, these yields together with the ratio of theoretical estimates of the direct photodisintegration (γ, α) and (γ, p) cross sections could be used to estimate the average number of α clusters in nuclei. Carver³⁶ made such estimates based on total α yields from V bombarded by 32 MeV bremsstrahlung, assuming only E1 photon absorption for both alphas and protons. Neither our data nor previous (γ, α) data^{18,23,36} establishes the correlation suggested above and therefore the principal value of this discussion is to establish rough ratios of A_3/A_0 for the (γ, p) and (γ, α) angular distributions which would be expected from direct photodisintegration. In spite of these cautions, we will obtain an estimate of the asymmetric component of our (e, p) and (e, α) yields which is consistent with the absorption of 35 MeV virtual photons based on our angular distributions and excitation data for $E_0 = 50, 75, 80, 110, \text{ and } 115$ MeV. We then assume this component is produced by direct photodisintegration by interference between photons of E1 and E2 multipolarities. Since we will compare portions of the α and proton energy spectra several MeV above the α Coulomb barrier, we assume the influence of the barrier in inhibiting the α yields should be negligible. If $(Z - 2N_\alpha)$ protons participate in the direct photodisintegration, the number of α clusters, N_α , predicted by the ratio of the α to proton E1-E2 interference cross sections is

$$N_\alpha \approx Z \frac{N_\alpha^0}{1 + 2N_\alpha^0}$$

$$\text{where } N_\alpha^0 = e_R M_R A_R / Y_R, \quad e_R = \frac{(e^{E1} e^{E2})_p}{(e^{E1} e^{E2})_\alpha}, \quad (19)$$

$$M_R = \frac{\langle f | O^{E1E2} | p, i \rangle \rho_p}{\langle f | O^{E1E2} | \alpha, i \rangle \rho_\alpha}, \quad A_R = \frac{\text{Atten}_p}{\text{Atten}_\alpha}, \quad Y_R = \left(\frac{Y_\alpha}{Y_p} \right)_{\text{Asymmetric}}$$

and Z is the nuclear atomic number. Here, e^{E1} and e^{E2} are the effective charges, O^{E1E2} is the E1E2 interference operator, and ρ_α and ρ_p are the density of states for the α and proton. The factor A_R has been included to account for the absorption of alphas and protons in the nucleus, although in a strict interpretation of the direct photodisintegration model, this factor should not appear. We use our ${}^9\text{Be}$ (e, α) and (e, p) data shown in Fig. (14) and estimates

of the effective number of α clusters in ${}^9\text{Be}$ obtained from $(p,p'\alpha)$ measurements to obtain an estimate of M_R in ${}^9\text{Be}$. Chant³⁷ estimates N_α^{Bc} is $.45 \pm .15$ from the analysis of ${}^9\text{Be}(p,p'\alpha)$ data. Based on our ${}^9\text{Be}(e,\alpha)$ and (e,p) energy spectra at 34° and 90° obtained with $E_0 = 110$ MeV, Y_R for alphas and protons of kinetic energies 20 ± 4 MeV, corresponding \approx to the absorption of 38 MeV photons for both alphas and protons, is $.27$. Measurements of Buchnea *et al*³⁸ show the ${}^9\text{Be}(\gamma,\alpha){}^5\text{He}$ reaction is \approx as probable as the ${}^9\text{Be}(\gamma,\alpha)n{}^4\text{He}$ reaction. The $\alpha+\alpha+n$ configuration is included in N_α^{Bc} ; however, since this configuration only contributes to the isotropic yields we reduce our estimate of N_α^{Bc} by $.5$. Using Eq. (19) with $A_R = 1$, and $N_\alpha^{\text{Bc}} = .22$ corresponding to $N_\alpha^{0(\text{Be})} = .06$,

$$M_R^{\text{Be}} \approx N_\alpha^{0(\text{Be})} \frac{4(N-Z)}{N} \left[\frac{(A-4)^2 + 8(Z-2)}{(A-1)^2 + (Z-1)} \right] \gamma_R \quad (20)$$

$\approx .11.$

This value for M_R^{Be} can be compared with a theoretical estimate obtained by assuming both the α and proton are bound in a square well in an relative S state. For such systems,

$$M_R^{\text{Be}} = 5 \sqrt{\frac{5S_p}{8S_\alpha} \left(\frac{k_\alpha}{k_p} \right)^3} \left[\frac{(k_p - S_p)^2 \cos \delta_{2p}}{(k_\alpha - S_\alpha)^2 \cos \delta_{2\alpha}} \right], \quad (21)$$

where S is the separation energy, and $\rho_{2\alpha}$, ρ_{2p} are the $(p, {}^8\text{Li})$ and $(\alpha, {}^5\text{He})$, $\ell = 2$, elastic scattering phase shifts.

To evaluate the attenuation factor, A_R , the mean free paths, λ_α and λ_p are needed. Igo *et al*² estimated the α mean free path in nuclear matter of 5% of the central nucleon density to be

$$\lambda_\alpha \approx [.0215 \ln(T_\alpha) + .318] \text{ fm}, \quad (22)$$

from data for T_α between 10 and 10^6 MeV. The proton mean free path obtained from an optical model analysis is³⁹

$$\lambda_p \approx 1.3 \sqrt{1 + \frac{68.6}{T_p}} \text{ fm}. \quad (23)$$

We estimate the attenuation factors for a spherical nucleus with a charge density parameterized by a Fermi distribution⁴⁰. The α distribution was assumed to be a Gaussian with a maximum located at a distance from the center of the nucleus suggested by Brink and Castro⁸. The proton distribution was taken to be the difference between the Fermi and α distributions. The relative attenuation factor, A_R is given by

$$A_R = \frac{(Z - 2N_\alpha) F_\alpha(\lambda_\alpha)}{[ZF_F(\lambda_p) - N_\alpha F_\alpha(\lambda_p)]} \quad (24)$$

This result is derived in Appendix II and values of $F_\alpha(\lambda_\alpha)$, $F_\alpha(\lambda_p)$, and $F_F(\lambda_p)$ are given in Table I. For a nucleus of mass number A ,

$$M_R^A = \sqrt[3]{\frac{8(A-4)}{5(A-1)}} M_R^{Be} \quad (25)$$

Values of $Y_R^{Ag} = .08$ for $T_\alpha = 19$ MeV and $Y_R^{Au} = .011$ for $T_\alpha = 23.5$ MeV were obtained from data shown in Figs. (15) and (16), and values of A_R are given in Table II. Finally we obtain an estimate based on the direct photodisintegration model of $N_\alpha = 6 \pm 3$ for ^{nat}Ag and 9 ± 4 for ^{197}Au .

V. CONCLUSIONS

The asymmetric component of our α -angular distributions cannot be understood in terms of existing statistical models. We do not know of completed pre-equilibrium or precompound model calculations⁴¹ which include a rigorous treatment of angular momentum. While such calculations are underway⁴², we seriously doubt that calculations which treat the fabrication of an alpha by sequential nucleon pickup can simultaneously reproduce our (e,p) and (e, α) angular distributions. Hence, we see no alternative to attributing the asymmetric component of our yields to a direct or semidirect process. A phenomenological model in which the incident virtual photon is absorbed by a quasideuteron²¹ resulting in a fast (p,n) pair which then interacts with the remaining nucleons via the same mechanisms as in (p, α) and (n, α) reactions seems to best fit our data. In this context, the arguments used to relate (p, α)^{1,33,45} and (n, α)¹⁸ reactions to nuclear surface clusters, can be used to relate our (e, α) yields to nuclear surface α clusters.

ACKNOWLEDGEMENTS

The author would like to thank members of the now defunct Nuclear Physics Group at NIST for helpful discussions.

TABLE I. Attenuation factors for alphas and protons in Ag and Au. The skin thickness parameter z of the Fermi charge distribution = .527 fm. Details of the calculation from which the attenuation factors were obtained are given in Appendix II.

c (fm)	T (MeV)	r_α (fm)	σ_α (fm)	$F_\alpha(\lambda_\alpha)$ $\times 10^3$	$F_\alpha(\lambda_p)$ $\times 10$	$F_F(\lambda_p)$ \times
5.20	19	6.78	1.0	.37	.64	.
5.20	19	6.78	2.0	.37	.63	.
5.20	19	7.89	2.0	.53	.63	.
5.20	19	6.78	.1	.23	.64	.
5.20	19	7.89	.1	1.10	.64	.
5.20	30	6.78	1.0	.40	.44	.
6.38	23.5	7.96	1.0	.28	.41	.
6.38	23.5	7.96	2.0	.28	.40	.
6.38	23.5	8.96	2.0	.40	.40	.
6.38	23.5	7.96	.1	.18	.36	.
6.38	23.5	8.96	.1	.86	.39	.
6.38	30	7.96	1.0	.29	.31	.

TABLE II. The ^{197}Au and ^{109}Ag (e, α) and (e, p) angular distribution asymmetries expressed as $\langle \text{asymmetry} \rangle = a_0 + a_1 \langle T \rangle$, where T is the kinetic energy, for E_0 50 and 110 MeV. The asymmetry is computed over the range of T indicated, first column labeled $\langle \text{asymmetry} \rangle$ and over an energy interval 10 MeV wide and starting at the T where the asymmetry becomes positive (second column labeled $\langle \text{asymmetry} \rangle$).

Reaction	Range (MeV)	a_0	a_1 /MeV	$\langle \text{asymmetry} \rangle$ Range	$\langle \text{asymmetry} \rangle$ $\Delta T = 10$ MeV	E_0 (MeV)
Au(e, α)	$16 < T_\alpha < 26$	$-.98 \pm .21$	$.06 \pm .01$	$.34 \pm .30$	$.32 \pm .29$	50
Au(e, α)	$16 < T_\alpha < 26$	$-.77 \pm .08$	$.044 \pm .004$	$.15 \pm .11$	$.22 \pm .11$	110
Au(e, p)	$8 < T_p < 23$	$-.42 \pm .04$	$.05 \pm .01$	$.36 \pm .16$	$.25 \pm .14$	50
Au(e, p)	$8 < T_p < 23$	$-.35 \pm .02$	$.039 \pm .001$	$.25 \pm .03$	$.20 \pm .02$	110
Ag(e, α)	$8 < T_\alpha < 26$	$-.38 \pm .03$	$.032 \pm .002$	$.16 \pm .04$	$.16 \pm .05$	50
Ag(e, α)	$8 < T_\alpha < 26$	$-.55 \pm .04$	$.048 \pm .003$	$.27 \pm .06$	$.24 \pm .06$	110
Ag(e, p)	$8 < T_p < 22$	$-.22 \pm .02$	$.03 \pm .01$	$.23 \pm .15$	$.15 \pm .13$	50
Ag(e, p)	$8 < T_p < 22$	$-.26 \pm .05$	$.04 \pm .01$	$.34 \pm .16$	$.20 \pm .13$	110

APPENDIX I.

Here $\mathfrak{R}(q)$ for an oscillator well {See Eq. (12)} is given.

$$\mathfrak{R}(q) = \frac{\mathfrak{R}_N(q)}{\mathfrak{R}_D(q)} \quad \text{where,}$$

$$\begin{aligned} \mathfrak{R}_N(q) &= p_o^2 [11p_o^2 + 4(q+p_c)(2q+p_c)] e^{-(2q+p_c)^2/p_o^2} \\ &\quad - [11p_o^4 + 4p_o^2(p_c^2 - p_{cq}) - 4p_{cq}(7p_o^2 + 4p_c^2)] e^{-p_c^2/p_o^2} \\ &\quad + 9\sqrt{2\pi}qp_o^3 \left[\text{erf}\left(\frac{2q+p_c}{\sqrt{2}p_o}\right) - \text{erf}\left(\frac{p_c}{\sqrt{2}p_o}\right) \right] \\ \mathfrak{R}_D(q) &= p_o^2 \{ [11p_o^2 + 4(q+p_c)(2q+p_c)] e^{-(2q+p_c)^2/p_o^2} \\ &\quad - [11p_o^2 - p_c(q+p_c)] e^{-p_c^2/p_o^2} \} \\ &\quad + 9\sqrt{2}qp_o^3 \left[\text{erf}\left(\frac{2q+p_c}{\sqrt{2}p_o}\right) + \text{erf}\left(\frac{p_c}{\sqrt{2}p_o}\right) \right]. \end{aligned} \tag{26}$$

The quantities p_o , q , and p_c are defined in the text. In deriving $\mathfrak{R}(q)$, we have assumed that nucleon momenta $p \gg p_c$ can be neglected.

APPENDIX II.

We calculated the α and proton attenuation factors by assuming an α particle distribution,

$$\rho_{\alpha}(r) \propto e^{-\left(\frac{r-r_{\alpha}}{\sigma_{\alpha}}\right)^2} \quad (27)$$

and normalized so that

$$\int \rho_{\alpha}(r) d^3r = 2N_{\alpha} \quad (28)$$

The overall charge distribution was given by a Fermi distribution

$$\rho_F(r) = \frac{\rho_{F_0}}{1 + e^{\frac{(r-z)}{z}}} \quad \text{normalized so that} \quad (29)$$

$$\int \rho_F(r) d^3r = Z.$$

The Fermi distribution parameters c and z were taken from Hahn et al.⁴² The proton charge distribution was $\rho_F(r) - \rho_{\alpha}(r)$. The parameter

$$r_{\alpha} = [z \ln(2) + c + R_{\text{nucleus}}] / 2 \quad (30)$$

as suggested by Brink and Castro³ and σ_{α} was treated as a free parameter subject to $\rho^{\alpha}(r) < \rho^F(r)$ and $2N_{\alpha} < Z$. The α and proton mean free paths were those given in the text. The attenuation factor, A_{α} , for alphas was then

$$\begin{aligned} A_{\alpha}(\lambda_{\alpha}) &= \frac{\iint_{\text{nuclear volume}} e^{-\frac{r-R}{\lambda_{\alpha}}} \rho_{\alpha}(r) d^3(r) d\Omega_R}{\iint_{\text{nuclear volume}} \rho_{\alpha}(r) d^3r d\Omega_R} \\ &= F_{\alpha}(\lambda_{\alpha}) \end{aligned} \quad (31)$$

The integration is over the volume and surface of a sphere of radius R such that $\rho_F(R) \ll .05\rho_{R0}$.

$$A_p(\lambda_p) = \frac{ZF_R(\lambda_p) - 2N_{\alpha}F_{\alpha}(\lambda_p)}{(Z - 2N_{\alpha})}. \quad (32)$$

The dependence of the attenuation factors on r_{α} and σ_{α} is explicitly displayed in Table II.

REFERENCES

1. D. H. Wilkinson, *Philos. Mag.* 4, 215 (1959); Proceedings of the Rutherford Jubilee International Conference, Manchester, 1961, ed. by J. B. Birks (Heywood and Co, Ltd., London, 1961) p. 339; Proceedings of the Kingston Conference on Nuclear Structure, Kingston, 1960, ed. by D. A. Bromley and E. W. Vogt (University of Toronto Press, Toronto, 1960) p. 20; Proceedings of the International School of Physics, "Enrico Fermi", ed. by T. E. O. Ericson (Academic Press Inc., London, 1967) p. 132; and Proceedings of the International Conference on Nuclear Structure, Tokyo, 1967, ed. by J. Sanada (*J. Phys. Soc. Jap. Supp.* 24, 469 (1968))
2. G. Igo, L. F. Hansen, and T. J. Gooding, *Phys. Rev.* 131, 337 (1963)
3. F. D. Becchetti, L. T. Chua, J. Jänecke, and A. M. Vandermolen, *Phys. Rev. Lett.* 34, 225 (1975)
4. L. Milazzo-Colli and G. M. Braga-Marcazzan, *Nucl. Phys.* A210, 297 (1973)
5. D. Bachelier, M. Bernas, O. M. Bilanink, J. L. Boyard, J. C. Jourdain, and P. Radvanyi, *Phys. Rev.* C7, 165 (1973)
6. H. E. Jackson, L. Meyer-Schützmeister, T. P. Wangler, R. P. Redwine, R. E. Segel, J. Tonn, and J. P. Schifter, *Phys. Rev. Lett.* 31, 1353 (1973); H. Ullrich, E. T. Boschitz, H. D. Engelhardt, and C. W. Lewis, *Phys. Rev. Lett.* 33, 433 (1974)
7. C. C. Chang, N. S. Wall, and Z. Fraenkel, *Phys. Rev. Lett.* 33, 1493 (1974)
8. D. M. Brink and J. J. Castro, *Nucl. Phys.* A216, 109 (1974)
9. T. T. S. Kuo, J. Blomqvist, and G. E. Brown, *Phys. Lett.* 31B, 93 (1970); G. E. Brown in Proceedings of the International Conference on Photonuclear Reactions and Applications, Asilomar-Pacific Grove, California, ed. by B. L. Berman, 1973 (available from the National Information Service, Springfield, VA. 22151, 1973) p. 57
10. A. Fleury and J. M. Alexander in Ann. Rev. Nucl. Sci., 24, 279 (1974), ed. by Emilio Segrè (*Ann. Rev. Nucl. Sci.*, Inc., Palo Alto, CA 94306
11. D. M. Skopik and W. R. Dodge, *Phys. Rev.* C6, 43 (1972)
12. J. F. Janni, Technical Report No. AFWF-TR-150, Air Force Weapons Laboratory, Research and Technology Laboratory, Air Force Systems Command, Kirkland Air Force Base, New Mexico

(available from the National Technical Information Service, Springfield, VA. 22151)

13. R. F. Frosch, J. S. McCarthy, R. E. Rand, and M. R. Yearian, Phys. Rev. 160 874 (1967)
14. H. Dubost, M. Lefoot, J. Peter, and X. Tarrago, Phys. Rev. B136, 1618 (1964)
15. J. O. Rasmussen, Rev. Mod. Phys. 30, 424 (1958)
16. W. Czyż, 131, 2141 (1963)
17. T. DeForest, Jr. and J. D. Walecka, Adv. Phys. 15, 1 (1966)
18. L. Meneghetti and S. Vitale, Nucl. Phys. 61, 316 (1965)
19. I. Dostrovsky, P. Rabinowitz, and R. Divins, Phys. Rev. 111, 1659 (1958); I. Dostrovsky, Z. Fraenkel, and G. Friedlander, Phys. Rev. 116, 683 (1959)
20. B. L. Berman, Atlas of Photoneutron Cross Sections Obtained with Monoenergetic Photons, 2nd ed., UCRL 75694, May 6, 1974
21. J. S. Levinger, Phys. Rev. 84, 43 (1951); J. Garvey, B. H. Patrick, J. G. Rutherglen, and I. L. Smith, Nucl. Phys. A70, 241 (1965)
22. G. Kraft, R. Kosiek, R. Mundhenke, and J. Winter, Nucl. Phys. A118, 25 (1968)
23. T. Ericson and V. Strutinski, Nucl. Phys. 8, 284 (1958); N. A. Keller and D. B. McConnell, Can. J. Phys. 50, 1554 (1972)
24. T. A. Gabriel and R. G. Alsmiller, Jr. Phys. Rev. 182, 1035 (1969)
25. J.-O. Adler, G. Andersson, and H. Å Gustafsson, Nucl. Phys. A223, 145 (1974)
26. W. Heitler, The Quantum Theory of Radiation (Oxford University Press, London, 1954) Third Edition, p. 242
27. J. J. Griffin, Phys. Rev. Lett. 17, 478 (1966); M. Blann Phys. Rev. Lett. 21, 1357 (1968)
28. C. K. Cline, Nucl. Phys. A193, 417 (1972)
29. E. Běták, P. Obložinský, I. Ribanský, Nucleonia 19, 687 (1974); I. Ribanský, P. Obložinský, and E. Běták, Nucl. Phys. A205, 545 (1973); P. Obložinský, E. Běták, I. Ribanský, Nucl.

- Phys. A226, 347 (1974)
30. F. E. Bertrand, R. W. Peelle, and C. Kalbach-Cline, Phys. Rev. C10, 1028 (1974)
 31. H. W. Bertini, G. D. Harp, and F. E. Bertrand, Phys. Rev. C10, 2472 (1974)
 32. F. E. Bertrand and R. W. Peelle, Phys. Rev. C8, 1045 (1973);
F. E. Bertrand and R. W. Peelle, ORNL Report No. 4460, 1969
 33. M. Lefort, J. P. Cohen, H. Dubost, and X. Tarrago, Phys. Rev. B139, 1500 (1966)
 34. J. S. Levinger, Phys. Rev. 84, 43 (1951)
 35. J. Eichler and H. A. Weidenmüller, Z. Phys. 152, 261 (1958)
 36. J. H. Carver, Proc. Phys. Soc. 27, 471 (1961)
 37. N. S. Chant, Proceedings of the Second International Conference on Clustering Phenomena in Nuclei, University of Maryland, April, 1975
 38. A. Buchnea, J. D. Irish, R. G. Johnson, B. J. Thomas, and K. G. McNeill, Bull Am. Phys. Soc., Series II, GN2, 17, 549 (1972)
 39. Norbert T. Porile, in Nuclear Chemistry I, 150 (L. Yaffe, ed., Academic Press, New York, 1968)
 40. B. Hahn, D. G. Ravenhall, and R. Hofstadter, Phys. Rev. 101, 1131 (1956)
 41. Herman Feshbach, Rev. Mod. Phys. 46, 1 (1974)
 42. Private communication, Herman Feshbach to W. R. Dodge
 43. A. Chevarier, N. Chevarier, A. Demeyer, G. Hollinger, P. Pertosa, and Tran. Minh Duc, Phys. Rev. C11, 886 (1975)

FIGURE CAPTIONS I.

- Fig. 1. Pulse height spectrum produced in a focal plane detector by the electrodisintegration of ${}^9\text{Be}$ at an electron bombarding energy of 110 MeV. The kinetic energy of the alphas and protons is 4.5 MeV.
- Fig. 2. ${}^{197}\text{Au}(e,\alpha)$ energy distributions. The \circ is for an electron bombarding energy, E_0 of 110 MeV. The \square is for $E_0 = 50$ MeV. The energy distributions also are A_0 .
- Fig. 3. Ratio of coefficients of a least-squares fit of ${}^{197}\text{Au}(e,\alpha)$ angular distributions for $E_0 = 110$ MeV to an expansion in Legendre polynomials which includes terms to $\ell = 3$.
- Fig. 4. Same as Fig. 3 except that $E_0 = 50$ MeV. The data were fit to an expansion in Legendre polynomials which included terms to $\ell = 2$.
- Fig. 5. ${}^{197}\text{Au}(e,p)$ energy distributions. The \circ is for an electron bombarding energy, E_0 of 110 MeV. The \square is for $E_0 = 50$ MeV. The energy distributions also are A_0 .
- Fig. 6. Ratio of coefficients of a least-squares fit of ${}^{197}\text{Au}(e,p)$ angular distributions for $E_0 = 110$ MeV to an expansion in Legendre polynomials which includes terms to $\ell = 3$.
- Fig. 7. Same as Fig. 6 except that $E_0 = 50$ MeV. The data were fit to an expansion in Legendre polynomials which included terms to $\ell = 2$.
- Fig. 8. ${}^{\text{nat}}\text{Ag}(e,\alpha)$ energy distributions. The target was naturally occurring Ag. The \circ is for $E_0 = 110$ MeV, and \square is $E_0 = 50$ MeV. The energy distributions also represent A_0 . Also see Fig. 3 for ${}^{197}\text{Au}(e,\alpha)$ energy distributions.
- Fig. 9. Ratio of coefficients of a least-squares fit of ${}^{\text{nat}}\text{Ag}(e,\alpha)$ angular distributions for $E_0 = 110$ MeV to an expansion in Legendre polynomials which includes terms to $\ell = 3$.
- Fig. 10. Same as Fig. 9 except that $E_0 = 50$ MeV. The data were fit to an expansion in Legendre polynomials which included terms to $\ell = 2$.
- Fig. 11. ${}^{\text{nat}}\text{Ag}(e,p)$ energy distributions. The target was naturally occurring Ag. The \circ is for $E_0 = 110$ MeV, and \square is for $E_0 = 50$ MeV. The energy distributions also represent A_0 .
- Fig. 12. Ratio of coefficients of a least-squares fit of ${}^{\text{nat}}\text{Ag}(e,\alpha)$ angular distributions for $E_0 = 110$ MeV to an expansion in Legendre polynomials which includes terms to $\ell = 3$.

- Fig. 13. Same as Fig. 12 except that $E_0 = 50$ MeV. The data were fit to an expansion in Legendre polynomials which included terms to $\ell = 2$.
- Fig. 14. ${}^9\text{Be}(e, \alpha)$ energy distributions. The \circ is for $E_0 = 110$ MeV, and the \square is for $E_0 = 50$ MeV. The energy distributions also represent A_0 .
- Fig. 15. ${}^{197}\text{Au}(e, \alpha)$ yields/MeV/sr/electron as a function of the bombarding energy E_0 , at angles between the direction of the emitted α and direction of the incident electron beam of 34° and 90° . The Δ are for an α kinetic energy, $T_\alpha = 16.0 \pm .9$ MeV, \circ for $T_\alpha = 17.9 \pm .9$ MeV, $\langle \rangle$ for $T_\alpha = 19.8 \pm .9$ MeV, ∇ for $T_\alpha = 21.7 \pm .9$ MeV, \square for $T_\alpha = 23.5 \pm .9$ MeV.
- Fig. 16. ${}^{241}\text{Ag}(e, \alpha)$ yields/MeV/sr/electron as a function of the bombarding energy E_0 , at angles between the direction of the emitted α and direction of the incident electron beam of 34° and 90° . The Δ are for an α kinetic energy, $T_\alpha = 14.4 \pm .9$ MeV, $\langle \rangle$ for $T_\alpha = 15.7 \pm .9$ MeV, ∇ for $T_\alpha = 16.9 \pm .9$ MeV, \blacksquare for $T_\alpha = 18.7 \pm .9$ MeV, \bullet for $T_\alpha = 20.4 \pm .9$ MeV.
- Fig. 17. ${}^{197}\text{Au}(e, p)$ and ${}^{241}\text{Ag}(e, p)$ yields/MeV/sr/electron as a function of the electron bombarding energy, E_0 , at 34° . The upper set of data points is for ${}^{197}\text{Au}(e, p)$ and here \circ is for $T_p = 10.9 \pm 1.4$ MeV, ∇ is for $T_\alpha = 13.7 \pm 1.4$ MeV, Δ is for $T_p = 19.3 \pm 1.4$ MeV, \square is for $T_p = 19.3 \pm 1.4$ MeV, $\langle \rangle$ is for $T_p = 24.0 \pm 1.4$ MeV. The lower set of data points is for ${}^{241}\text{Ag}(e, p)$ and here \circ is for $T_p = 7.5 \pm .9$ MeV, \square is for $T_p = 9.2 \pm .9$ MeV, $\langle \rangle$ is for $T_p = 10.9 \pm .9$ MeV, \bullet is for $T_p = 12.6 \pm .9$ MeV, Δ is for $T_p = 18.2 \pm 1.3$ MeV and ∇ if for $T_p = 20.8 \pm 1.3$.
- Fig. 18. ${}^9\text{Be}(e, \alpha)$ yields/MeV/sr/electron as a function of the bombarding electron energy, E_0 , at 34° . The \circ refer to $T_\alpha = 6.7 \pm 1.9$ MeV, \square refer to $T_\alpha = 8.5 \pm 1.9$ MeV, ∇ refer to $T_\alpha = 10.4 \pm 1.9$ MeV, $\langle \rangle$ refer to $T_\alpha = 12.3 \pm 1.9$ MeV, Δ refer to $T_\alpha = 14.2 \pm 1.9$ MeV, \star refer to $T_\alpha = 16.0 \pm 1.9$ MeV, \bullet refer to $T_\alpha = 14.2 \pm 1.9$ MeV.
- Fig. 19. ${}^{197}\text{Au}$ $d\sigma(k)/d\Omega$ derived from excitation data shown in Figs. 14 to 17. The curve labeled (a) is the $d\sigma(k)/d\Omega$ for protons with kinetic energy $T_p = 23 \pm 1$ MeV at $\theta_p = 34^\circ$. The curves labeled (b) and (c) are $d\sigma(k)/d\Omega$ for alphas at 90° and 34° , respectively.
- Fig. 20. ${}^{241}\text{Ag}$ (e, p) and (e, α) cross sections. The \square is the proton $d\sigma(k)/d\Omega$, and \circ is the alpha $d\sigma(k)/d\Omega$ at the indicated α kinetic energies for $\theta_\alpha = 90^\circ$.

- Fig. 21. The number of recoil alphas with energies above a cutoff kinetic energy, T_{\min} , from elastic ${}^4\text{He}(e,e')\alpha$ as a function of the incident electron energy, E_0 .
- Fig. 22. The number of recoil protons with energies above a cutoff kinetic energy, T_{\min} , from elastic ${}^4\text{H}(e,e')p$ as a function of the incident electron energy, E_0 .
- Fig. 23. Comparison of ${}^{197}\text{Au}(e,p)$ energy distributions for $E_0 = 50$ (\square) and 110 MeV (\circ) with the predictions of the statistical model described in the text. The theoretical prediction for the peak of the energy distribution had to be multiplied by 4.26 to bring the prediction into agreement with experiment.
- Fig. 24. Comparison of ${}^{197}\text{Au}(e,\alpha)$ energy spectra for $E_0 = 50$ (\square) and 110 MeV (\circ) with the predictions of the statistical model described in the text and with the same input data and parameters used in the calculation for the ${}^{197}\text{Au}(e,p)$ cross section shown in Fig. 23. In this case, the theoretical prediction had to be multiplied by 3.1×10^{-3} to bring the peak prediction into agreement.
- Fig. 25. Comparison of $\sigma/\text{eq. quantum}$ obtained from this work \circ and from 500 MeV bremsstrahlung, histogram, Ref. 16. The smooth curve is a calculation taken from Ref. 16 and described in the text.

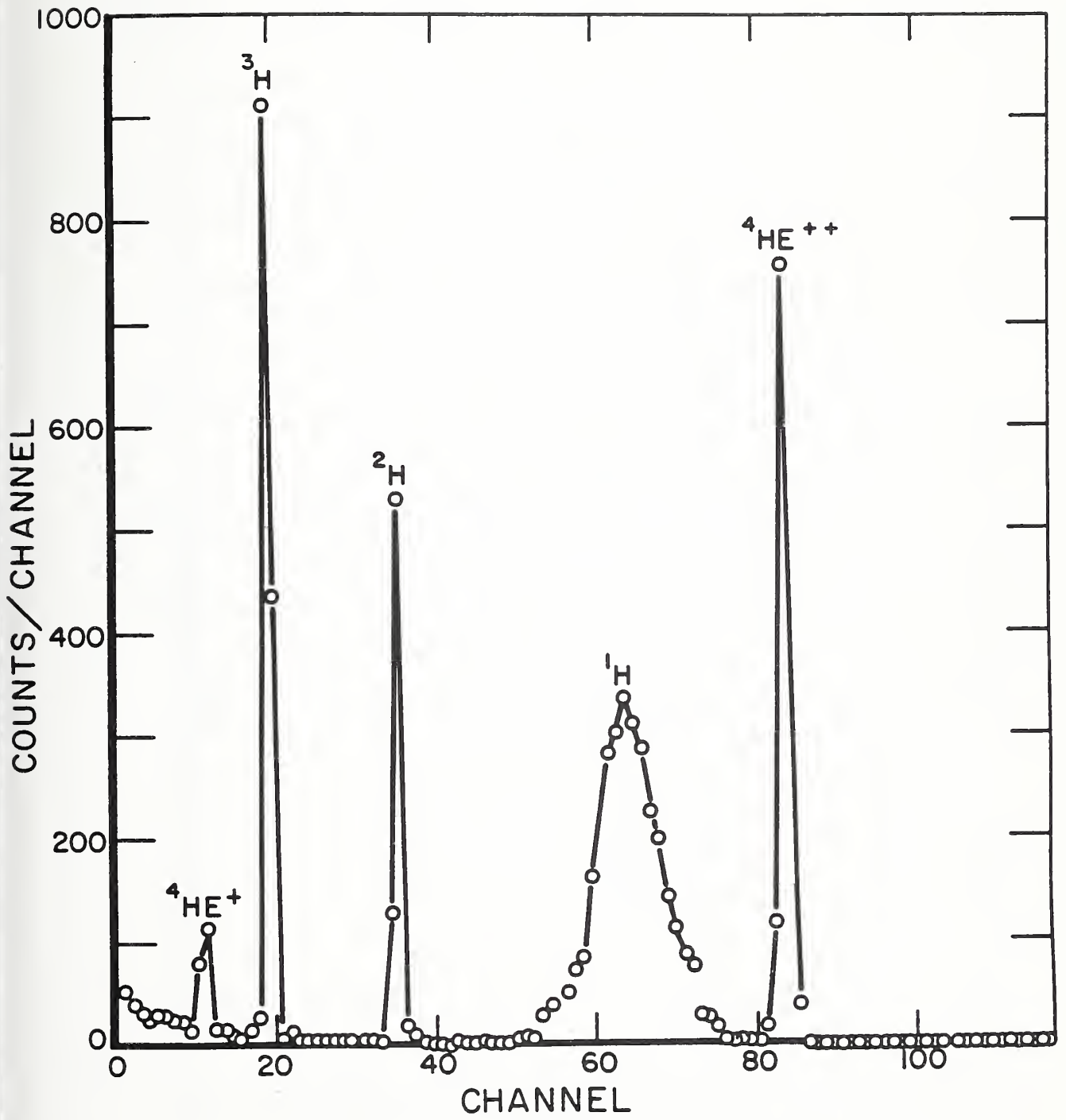
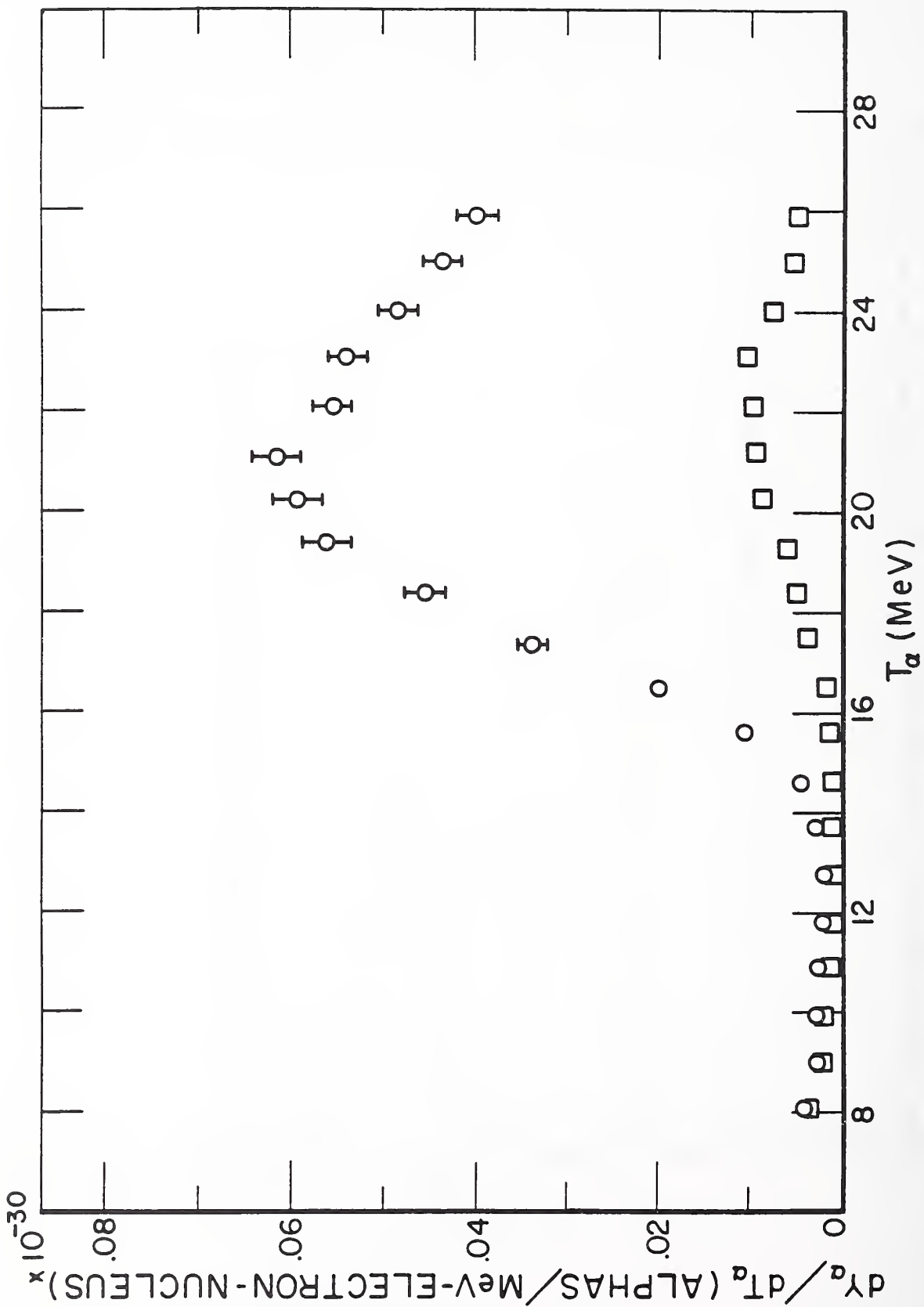


Fig. 1



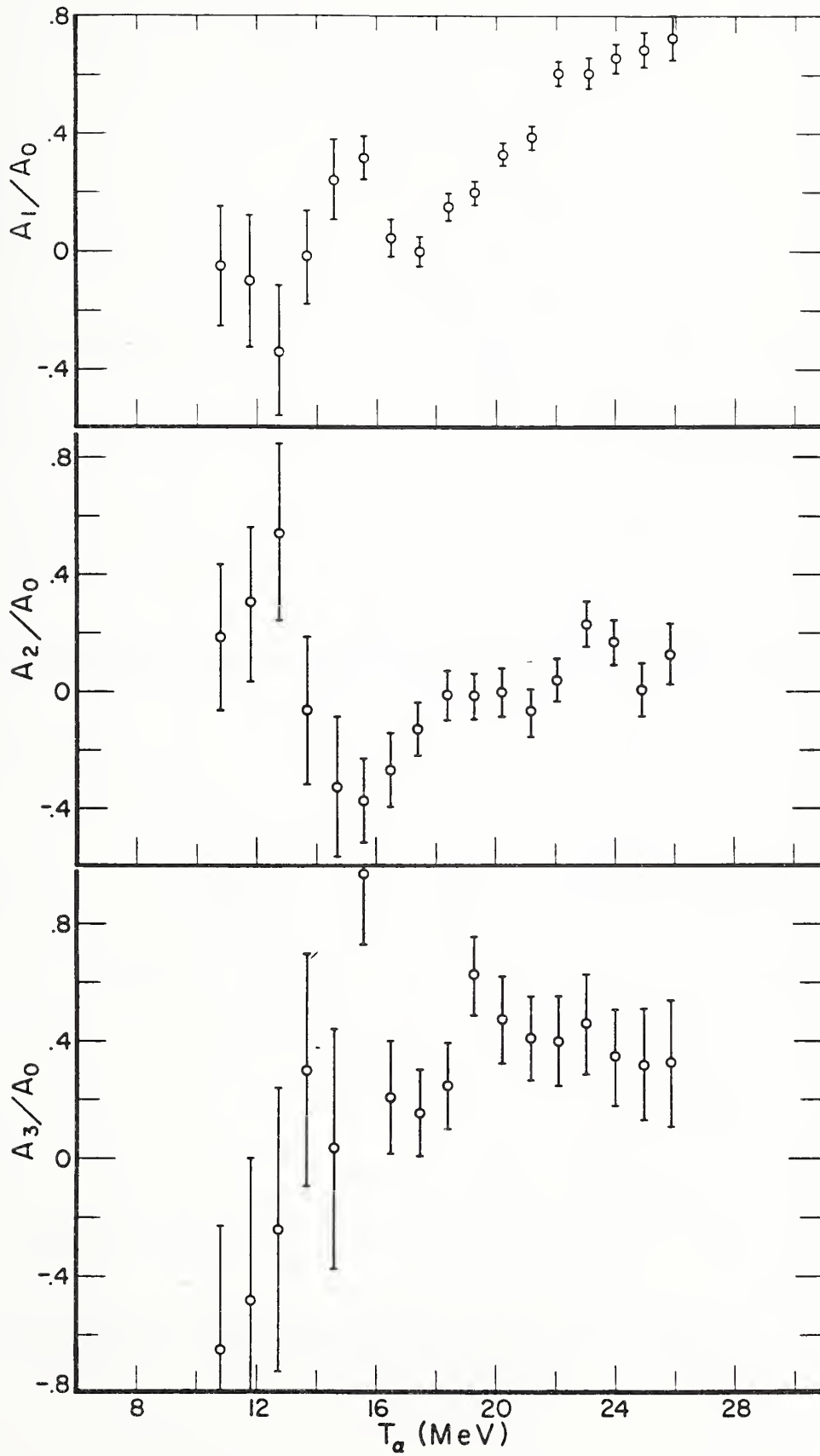
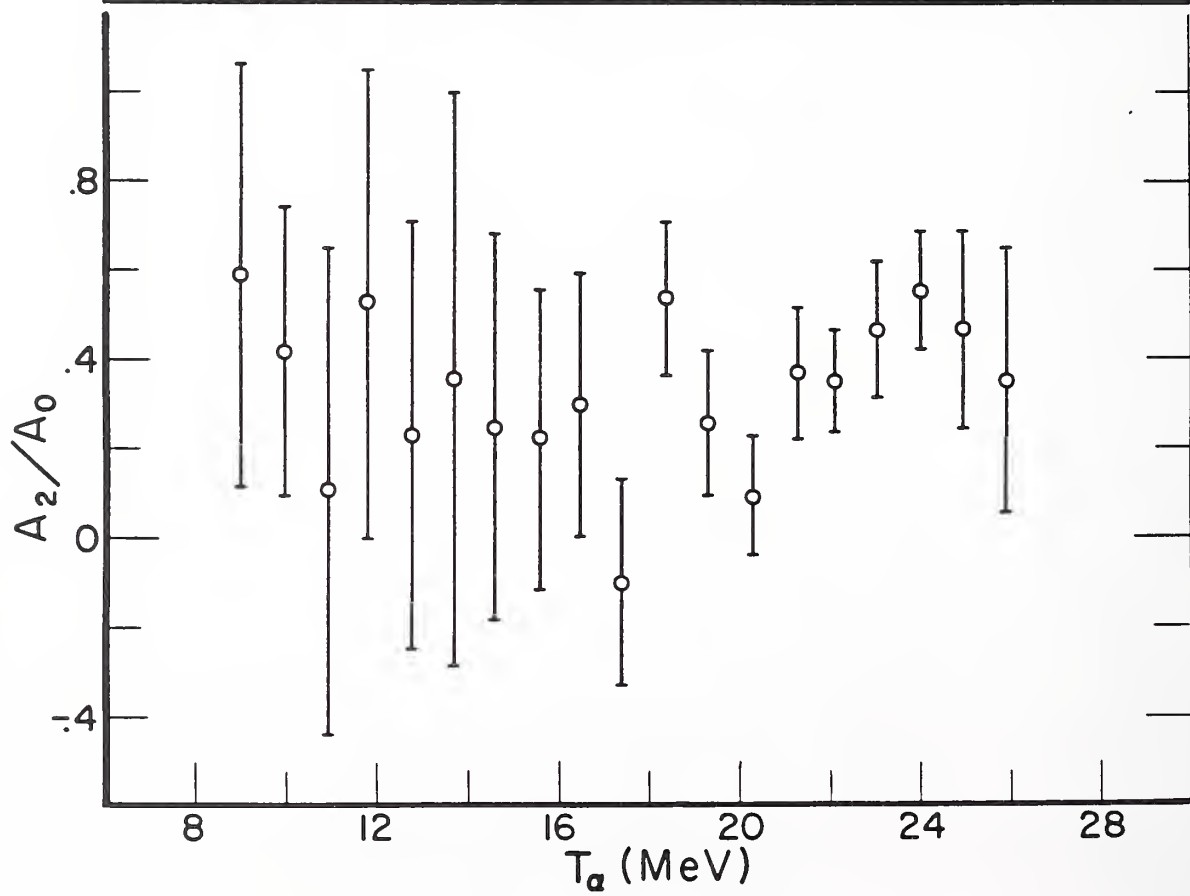
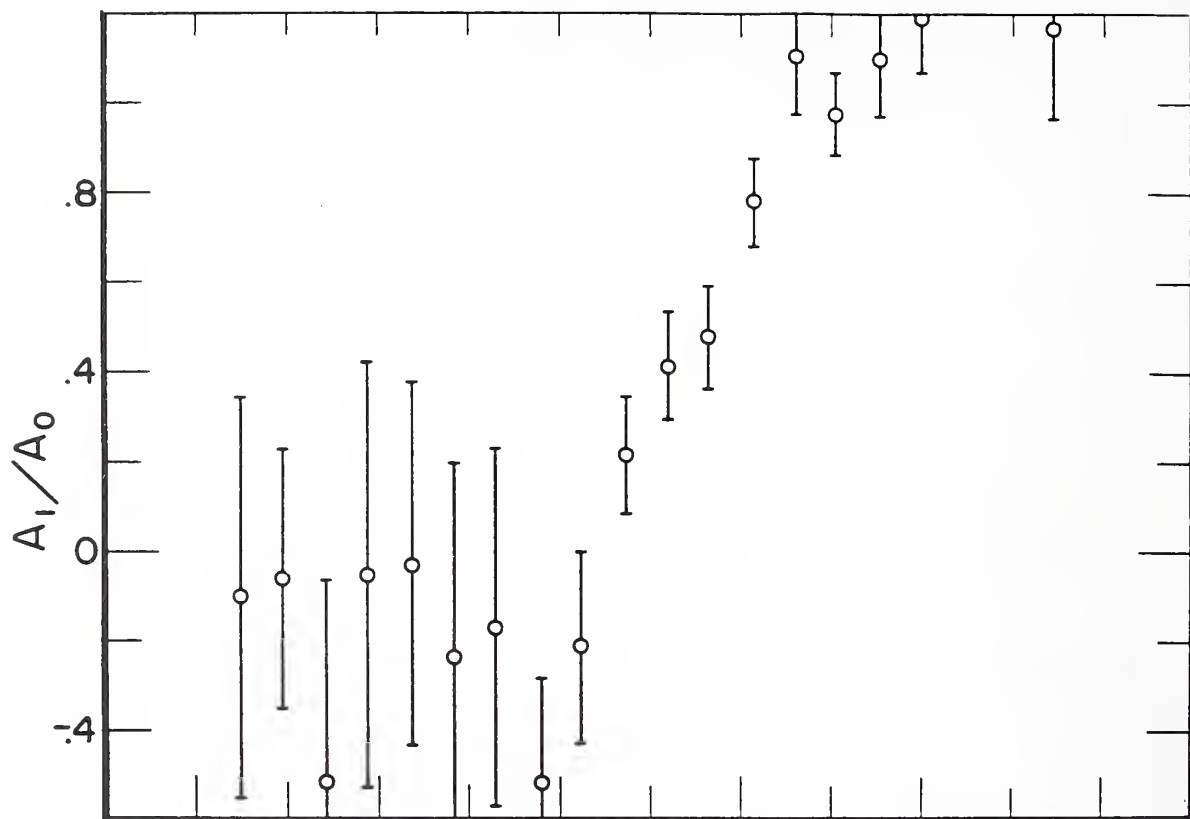
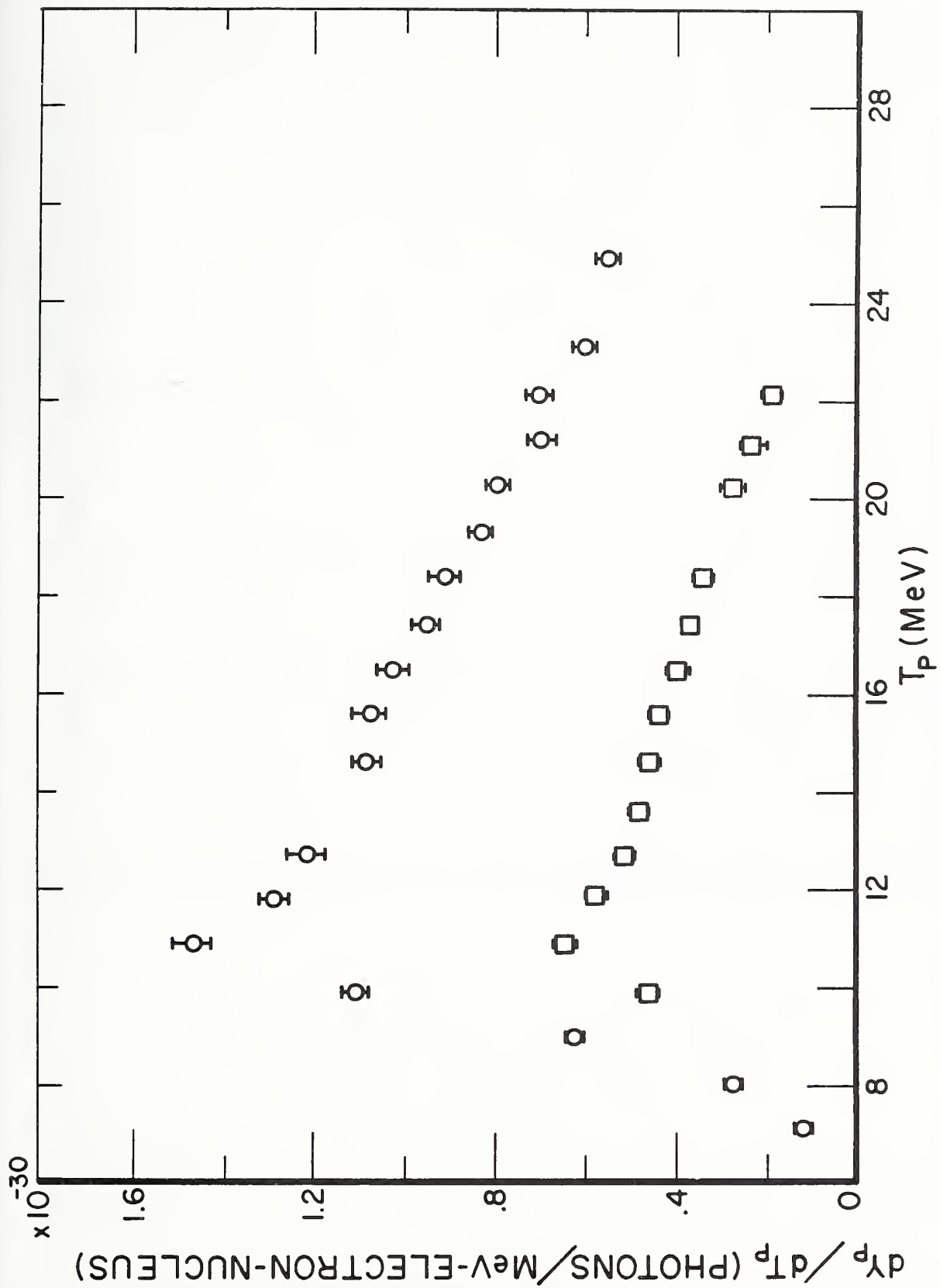
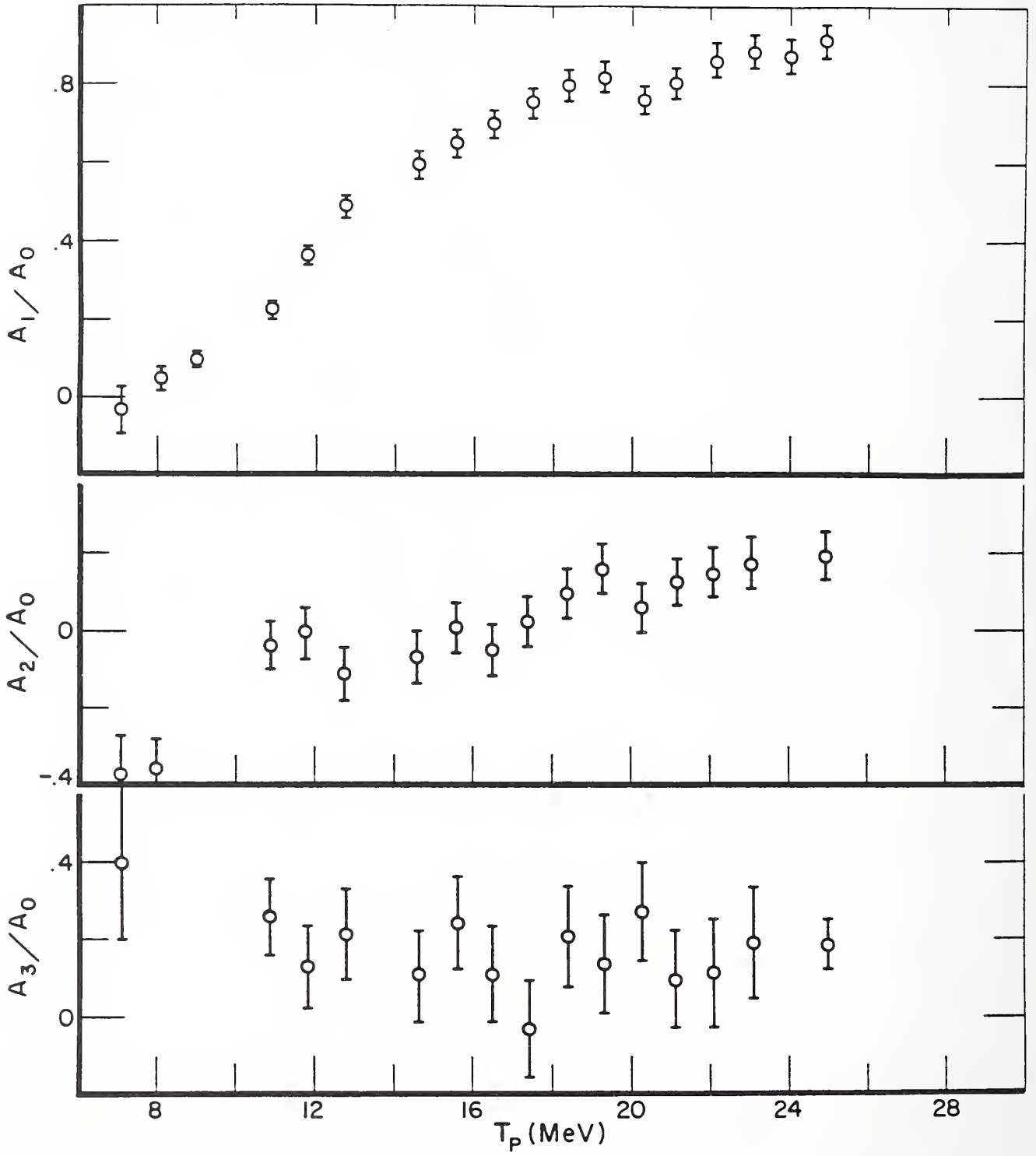
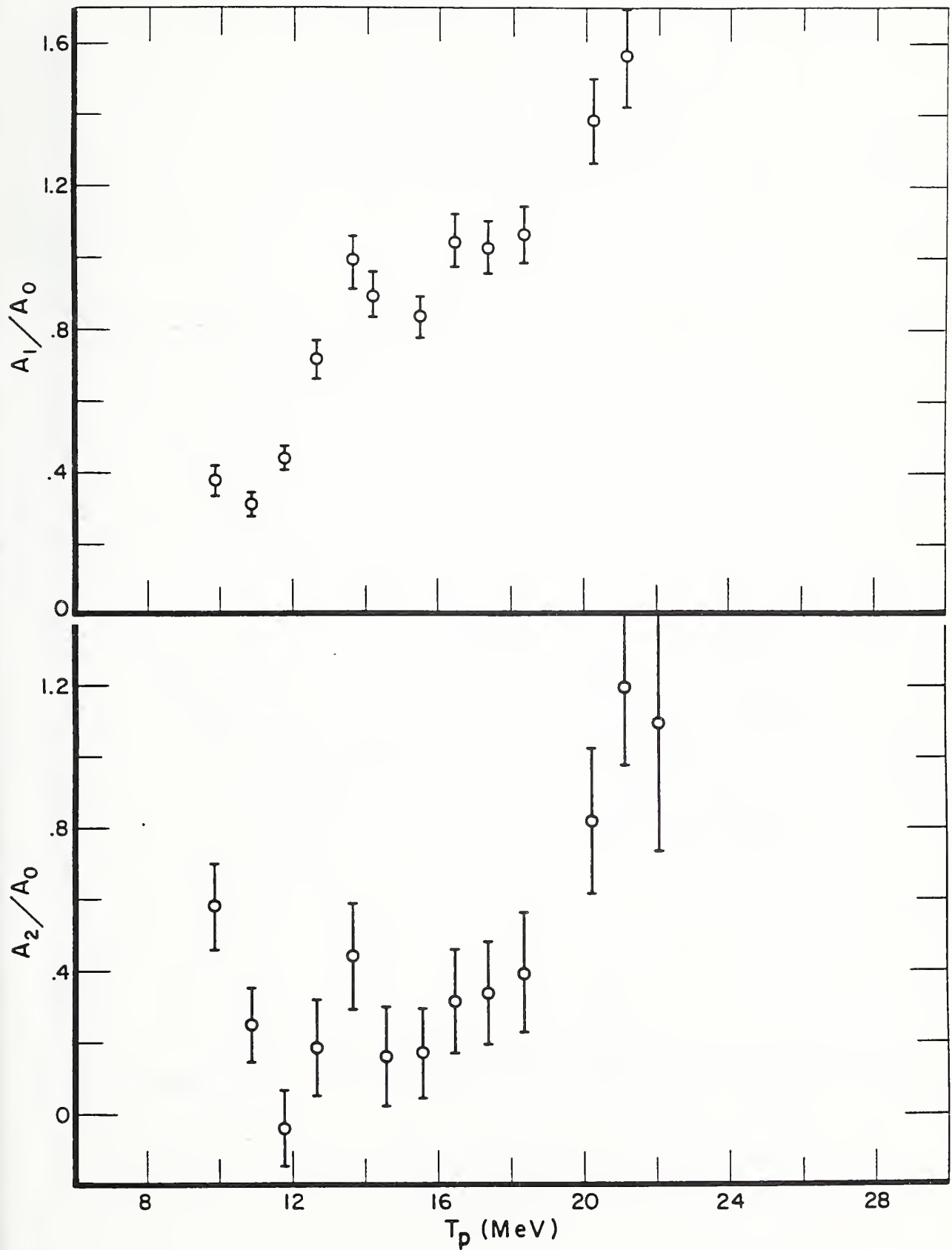


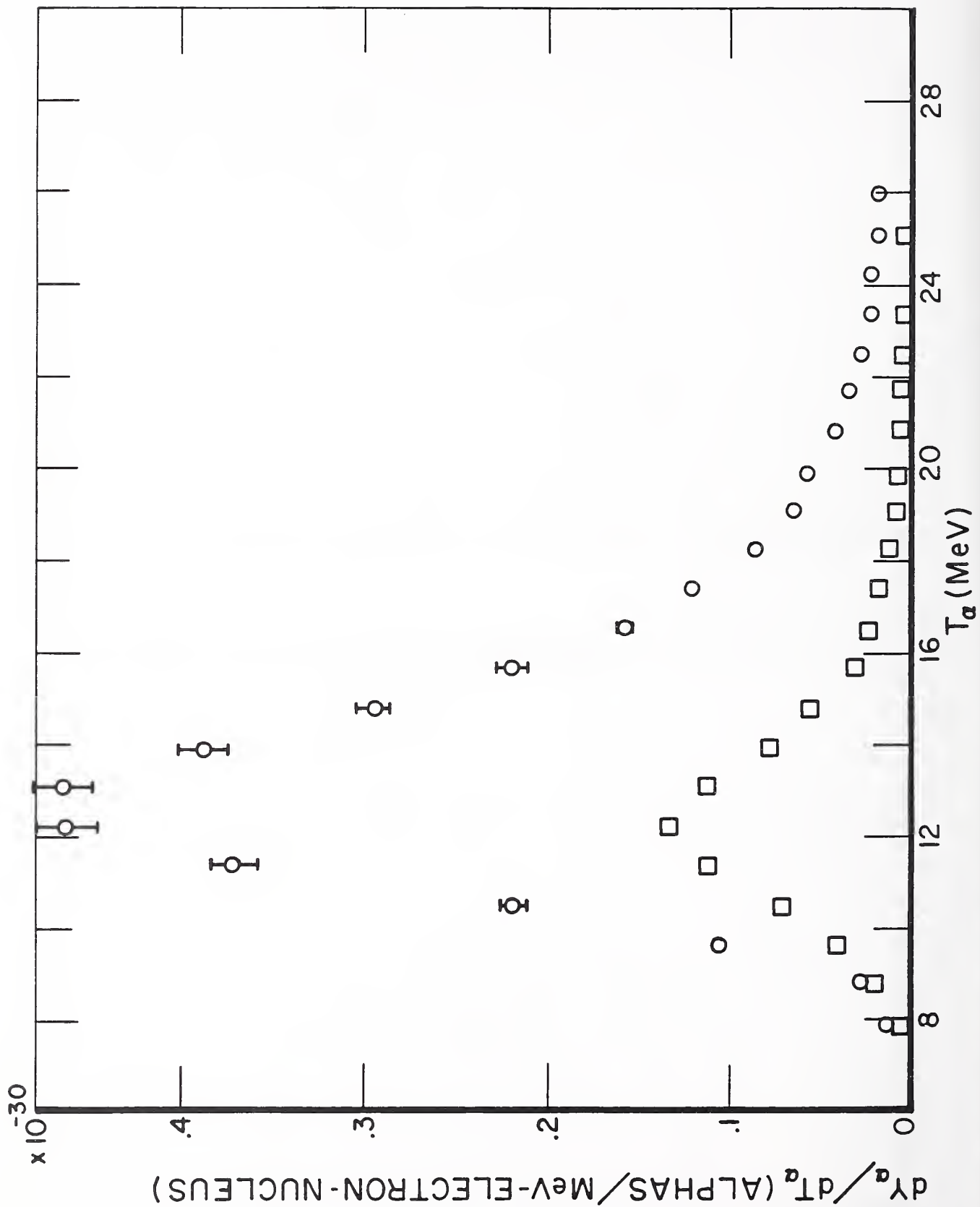
Fig. 3

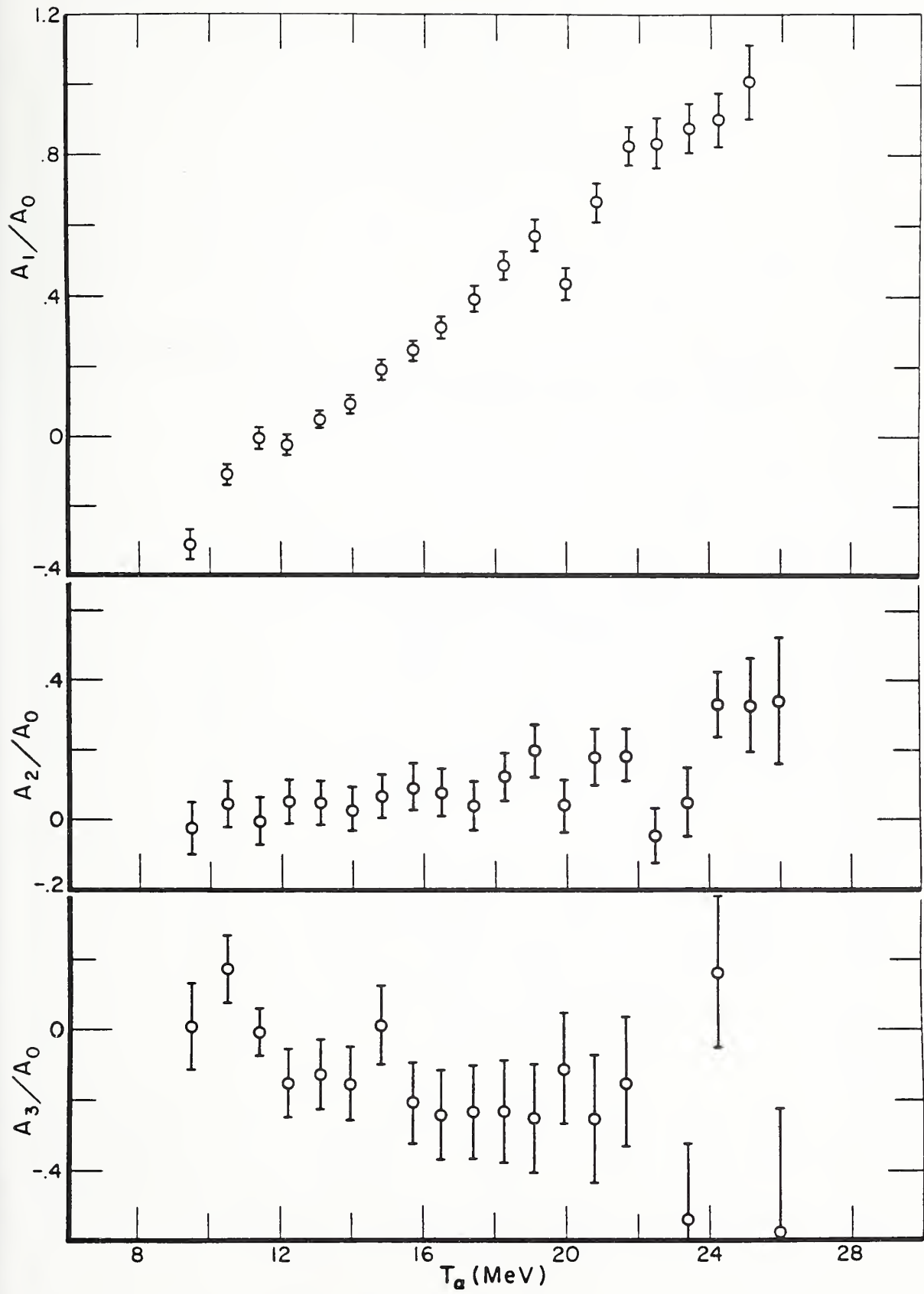


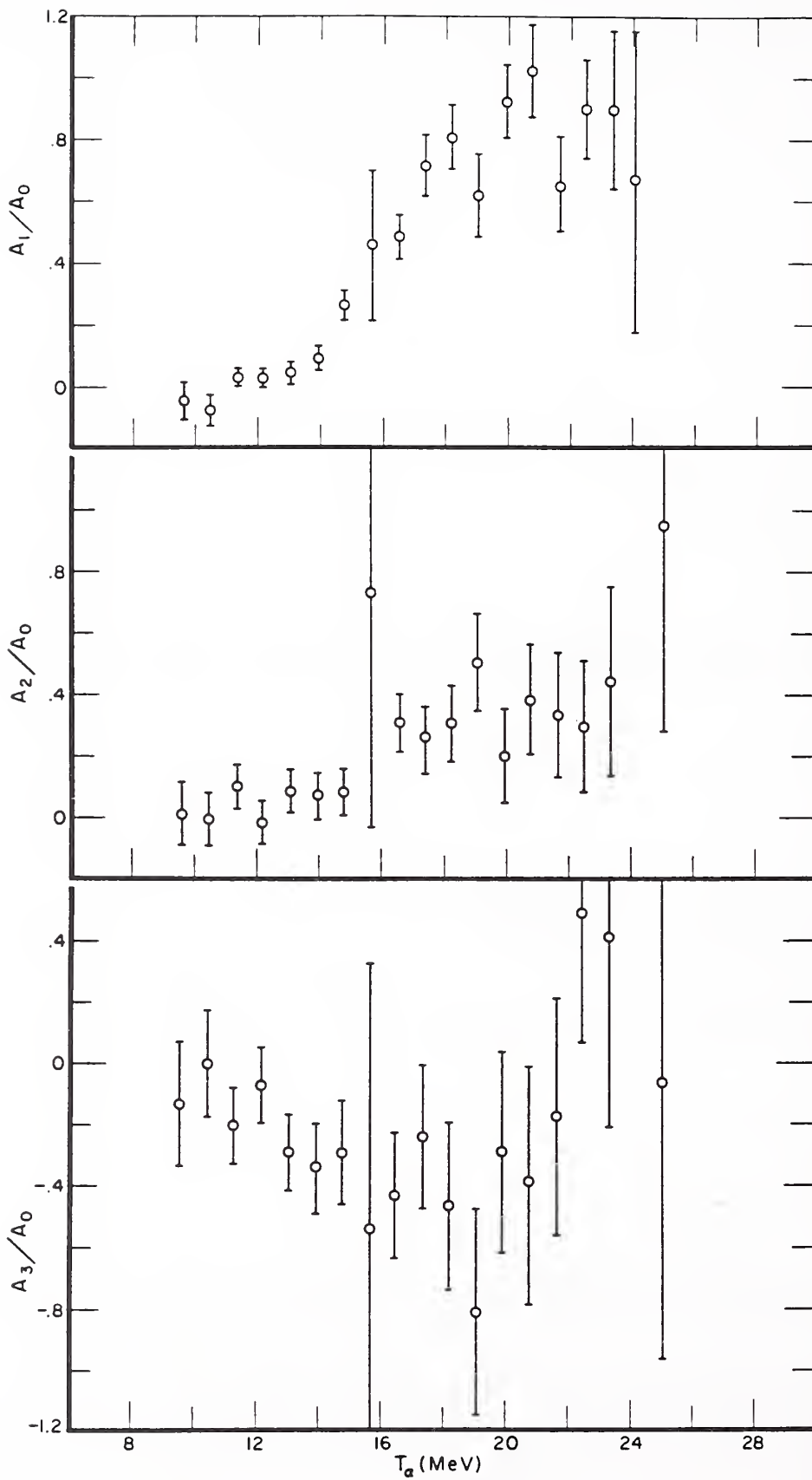




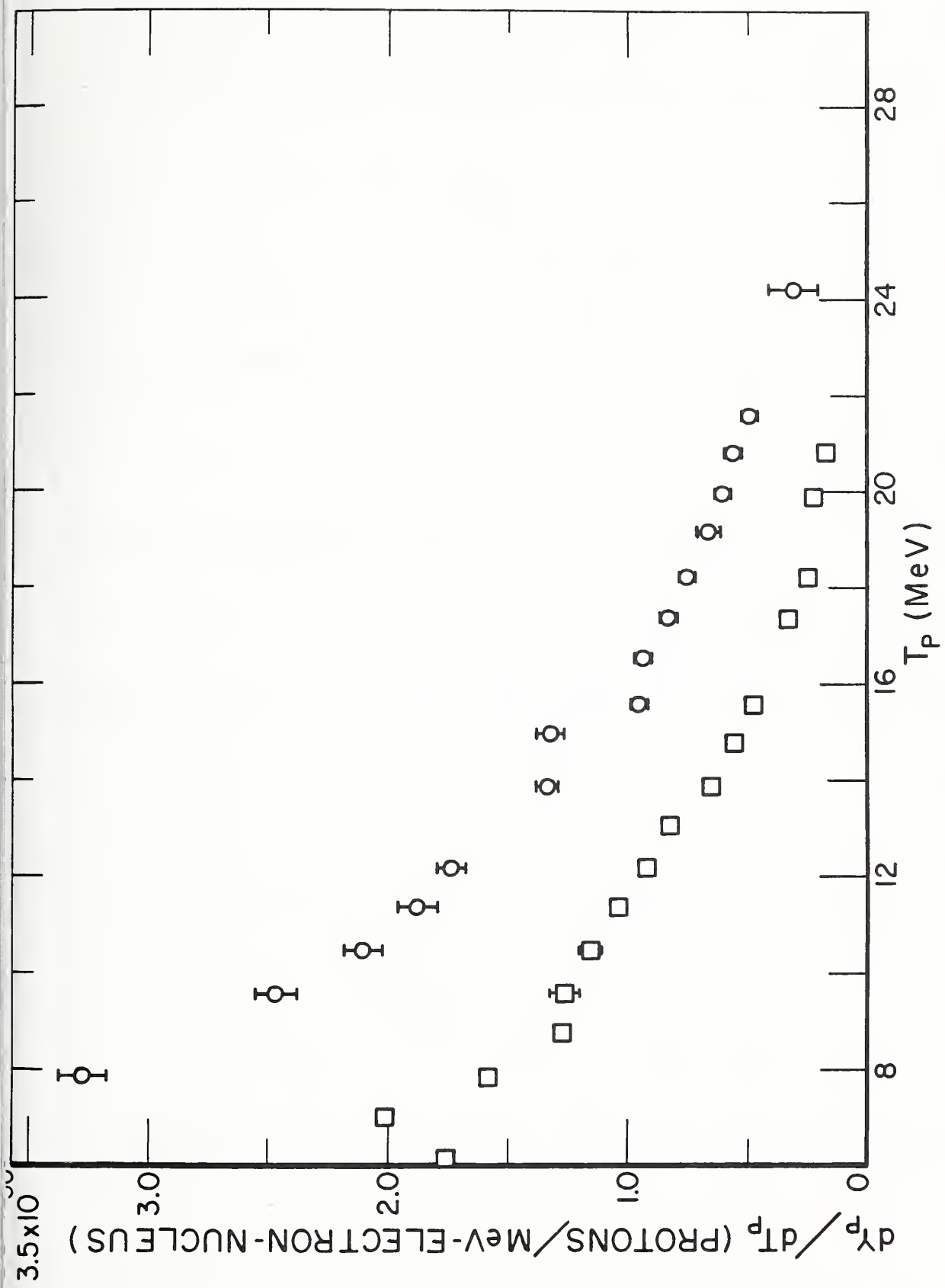


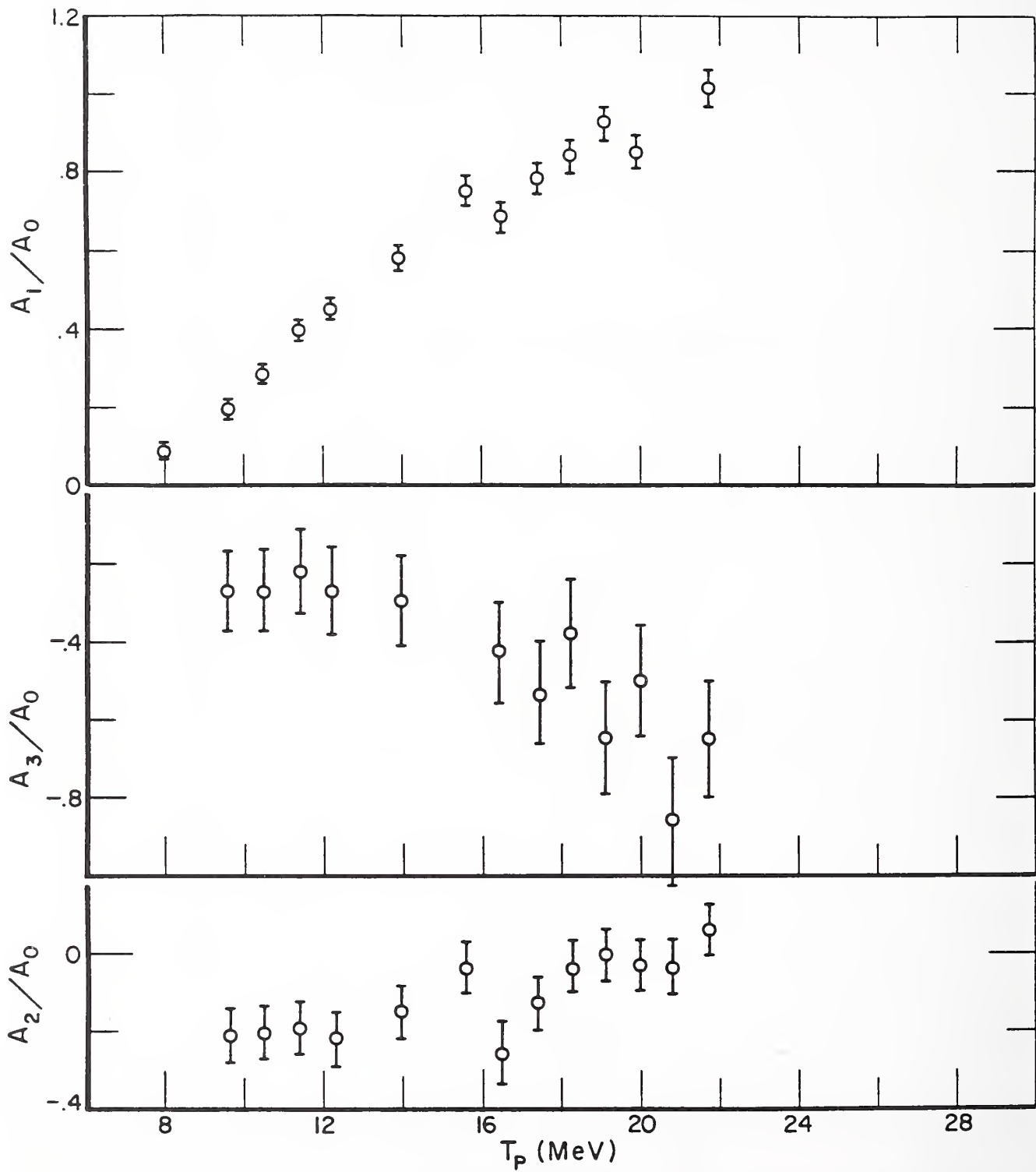






3.5x10⁶





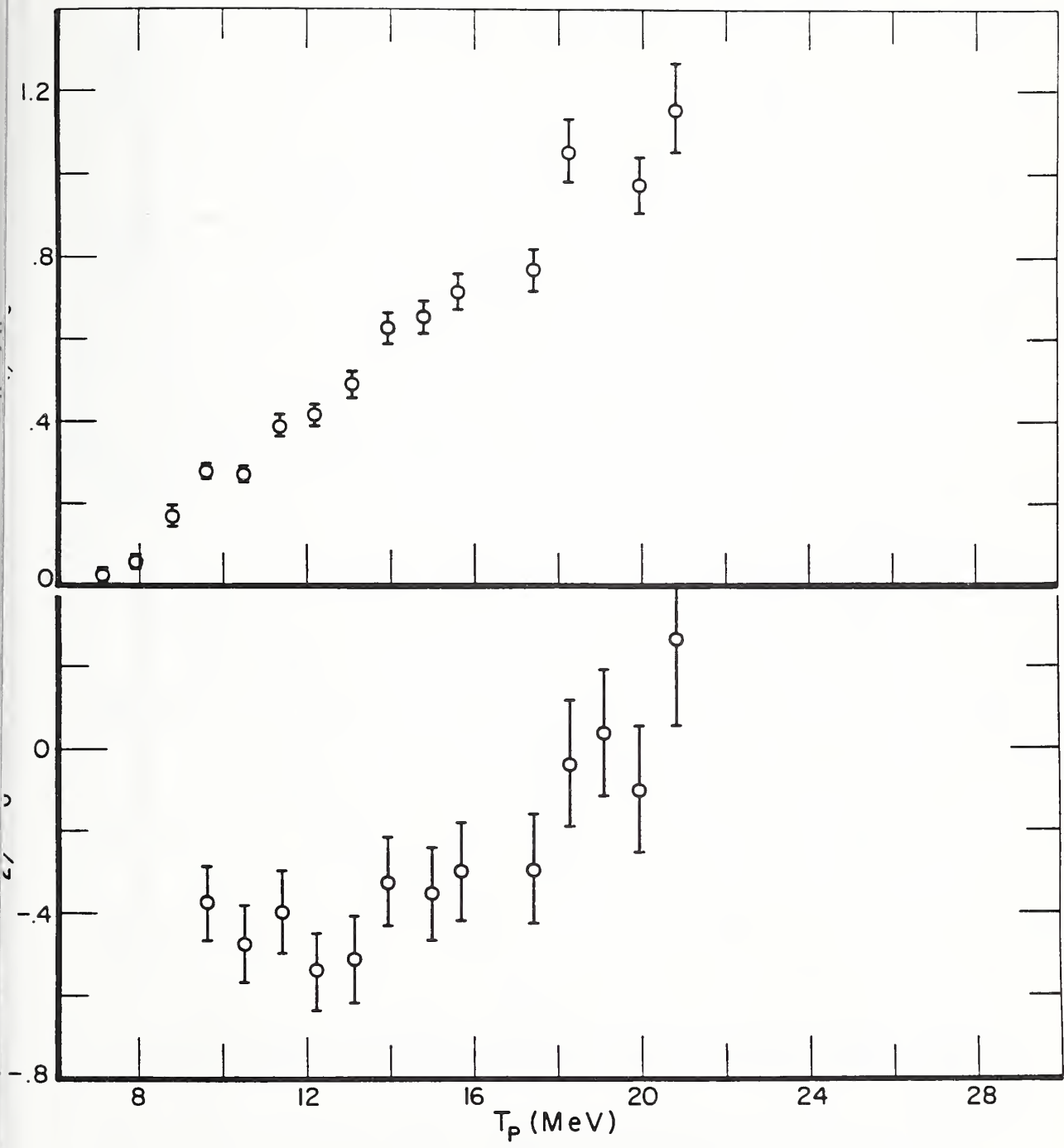
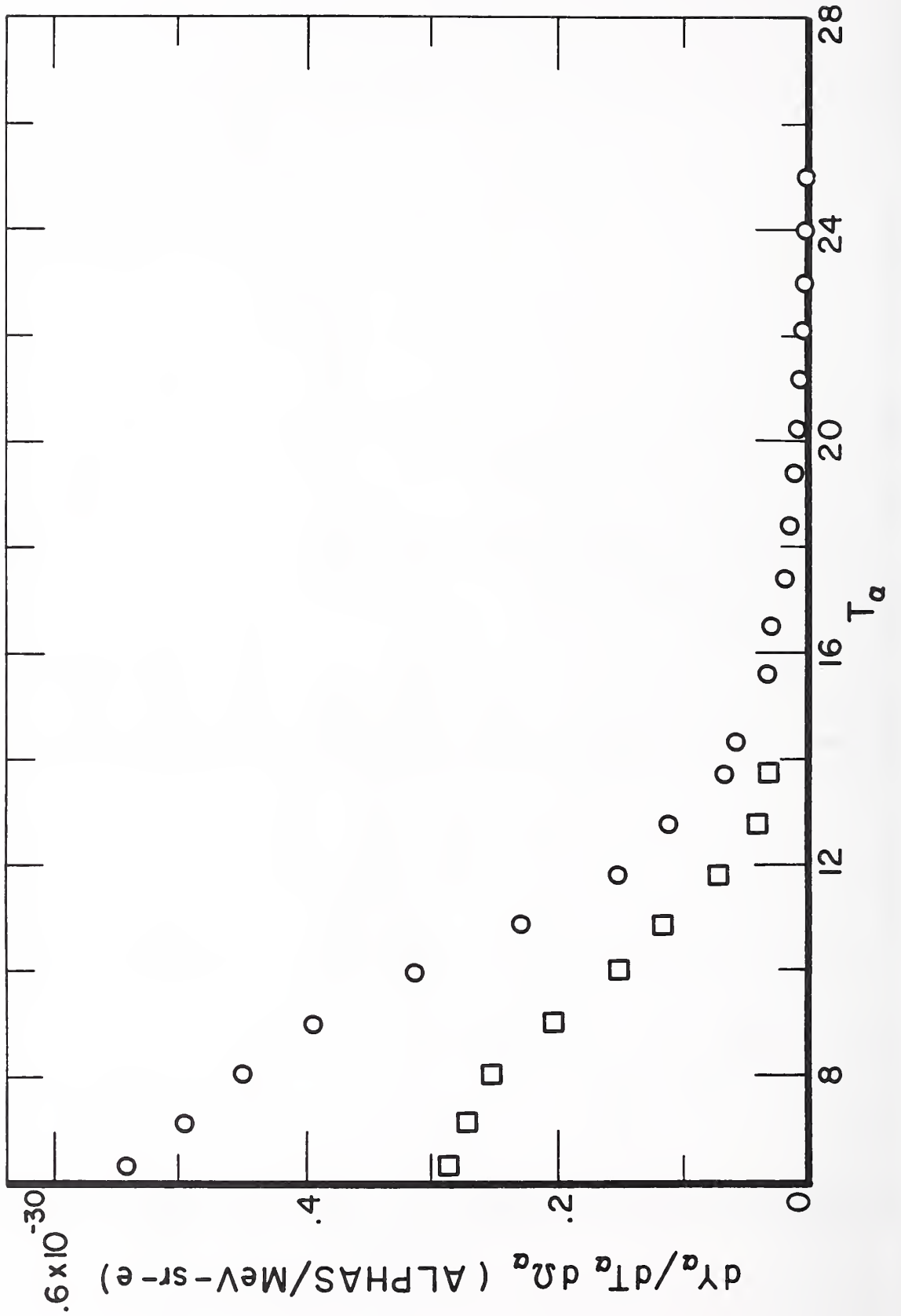


Fig. 13



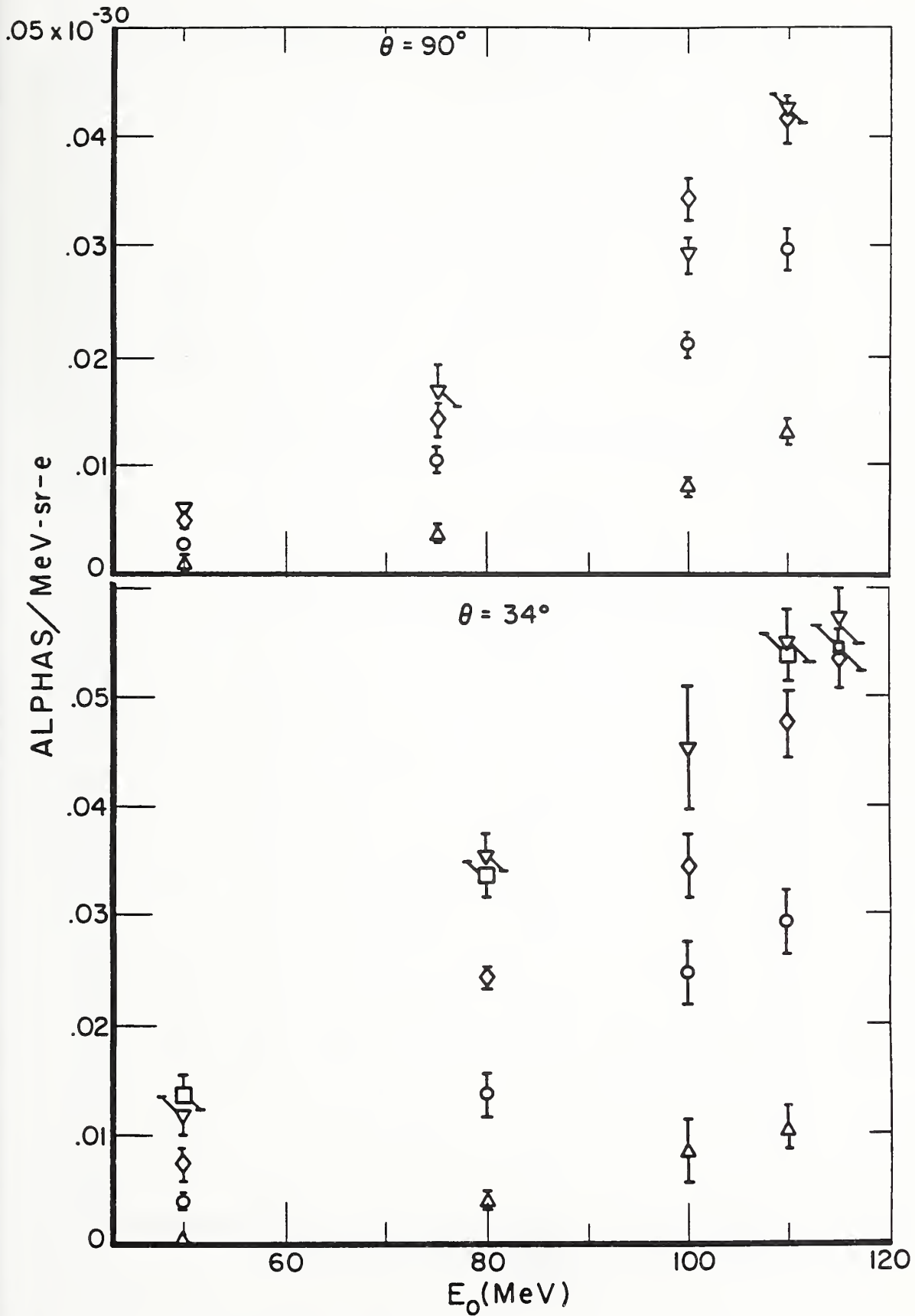


Fig. 15

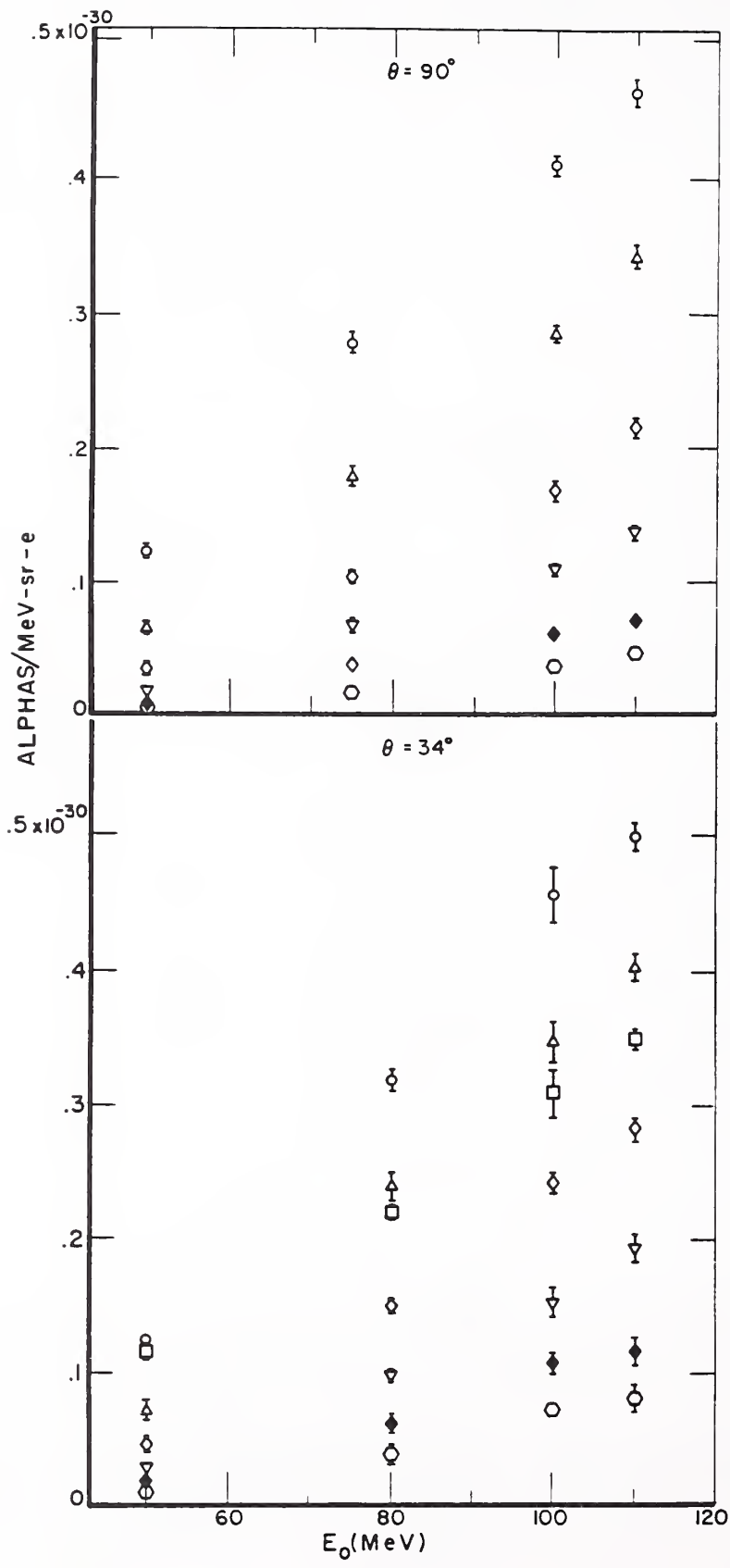


Fig. 1

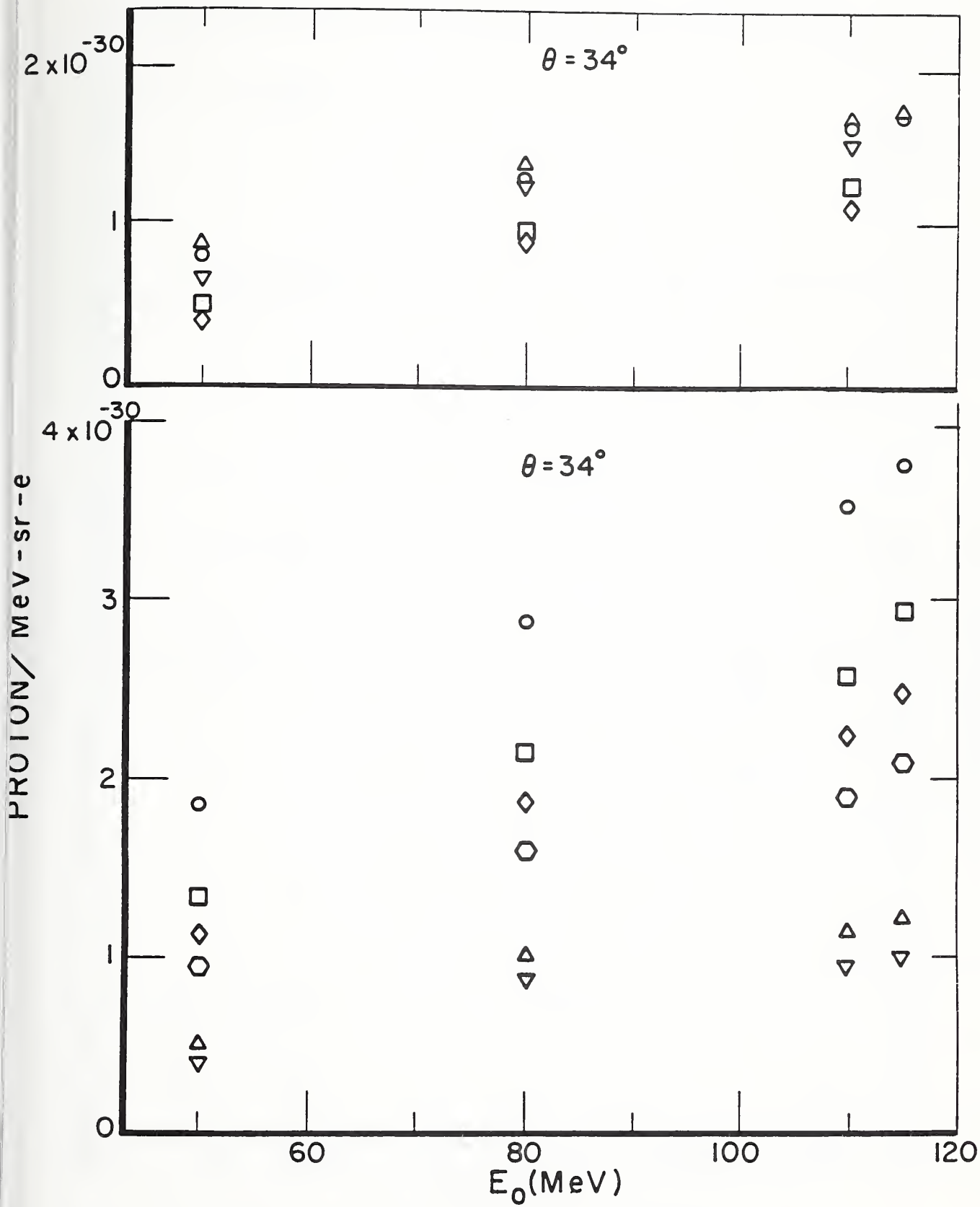
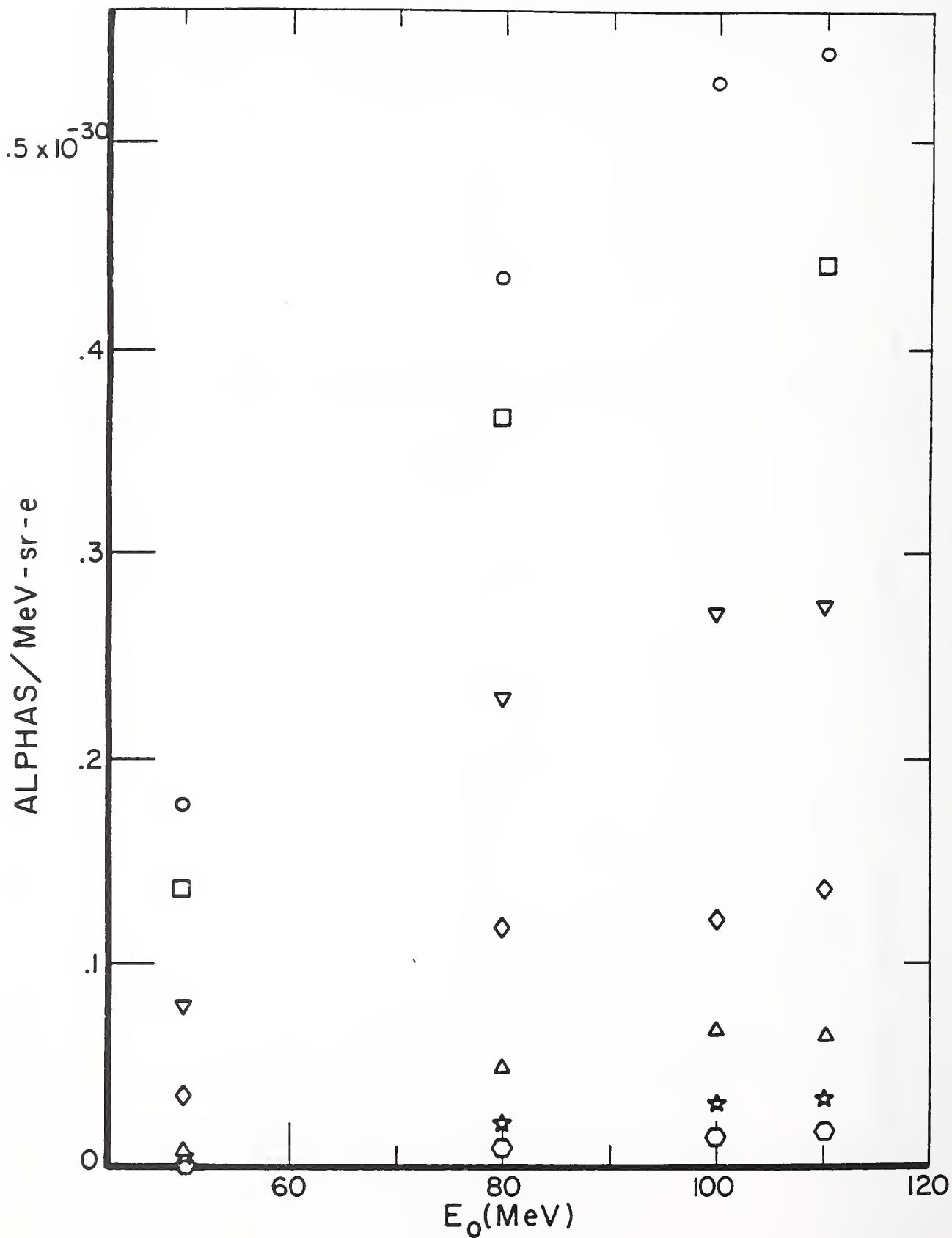
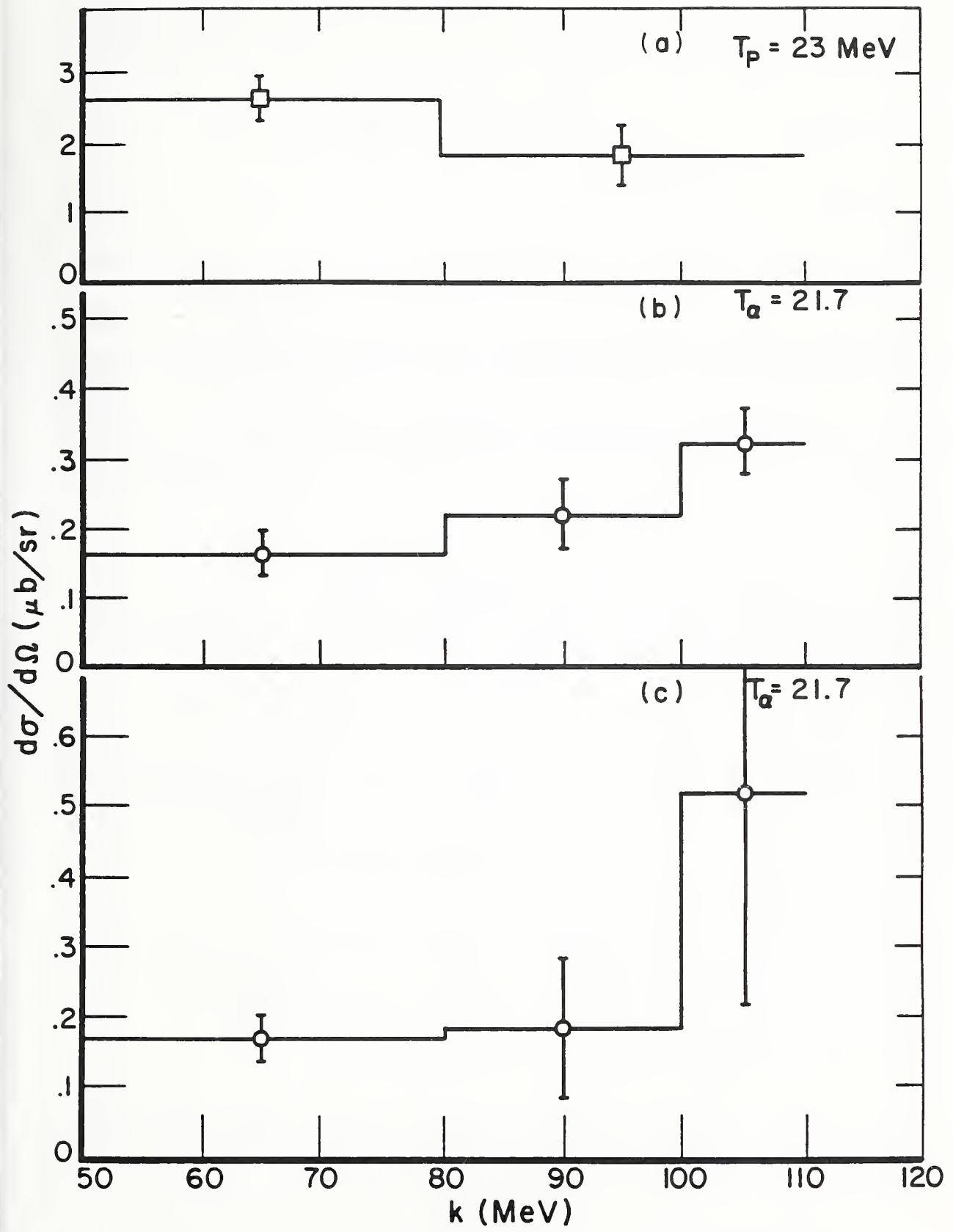
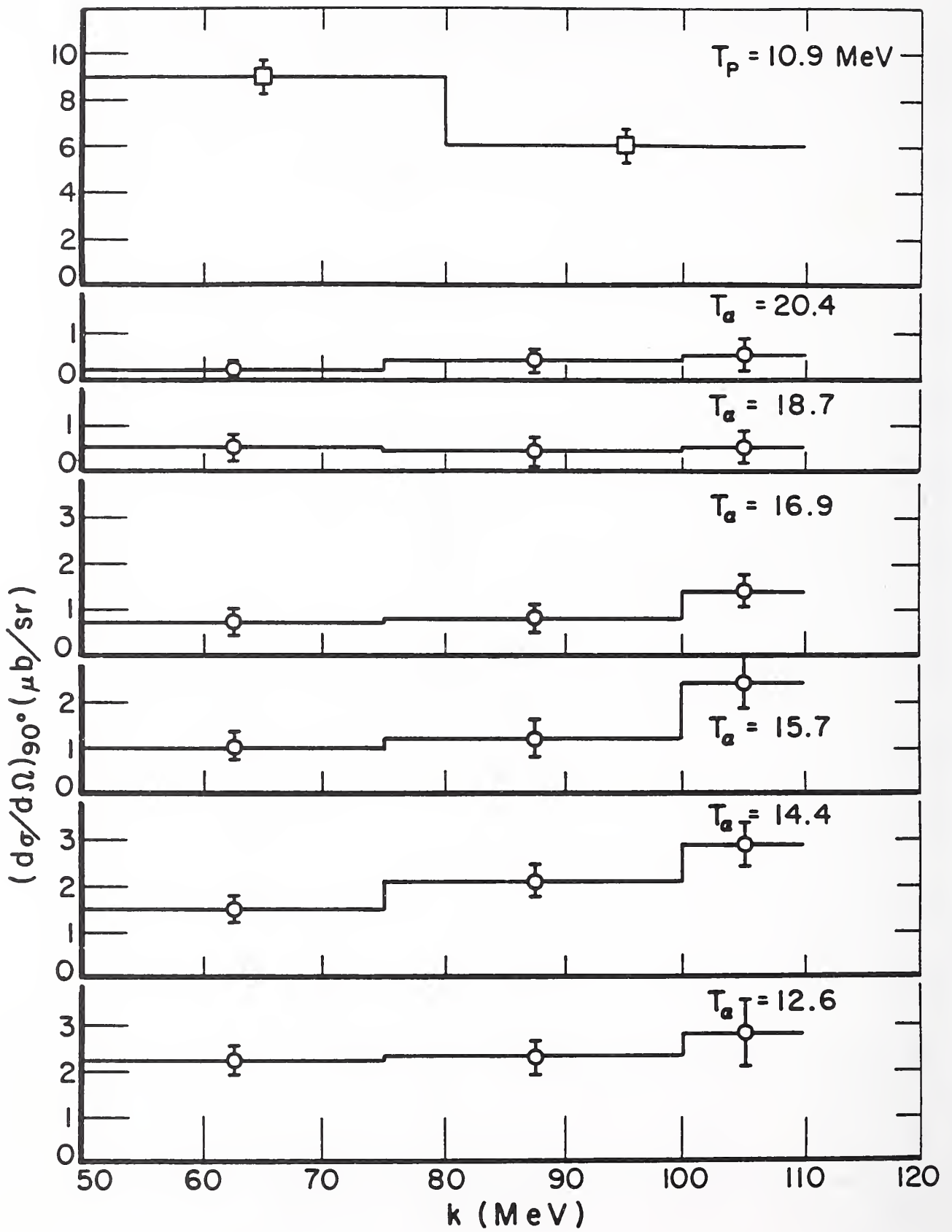


Fig. 17







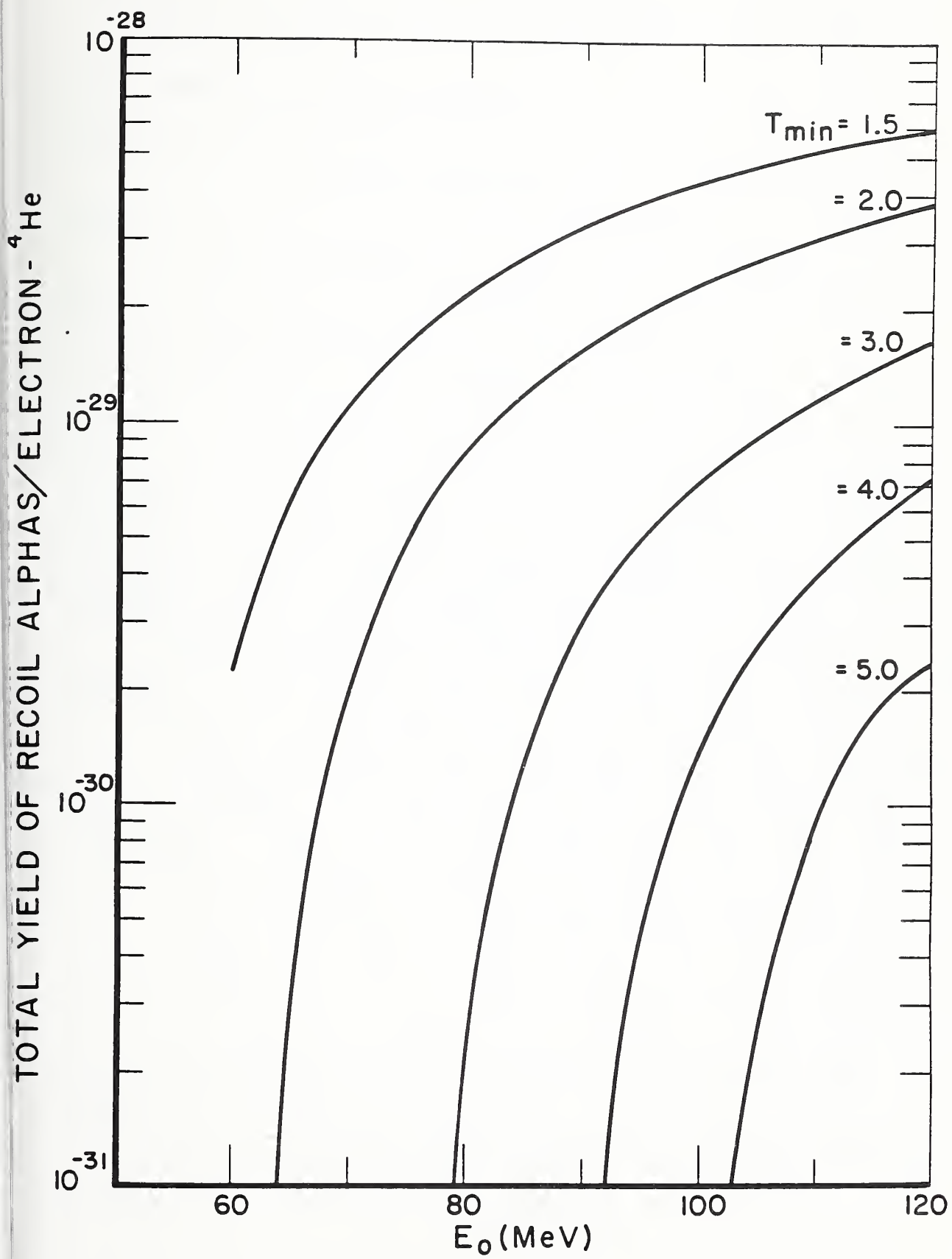
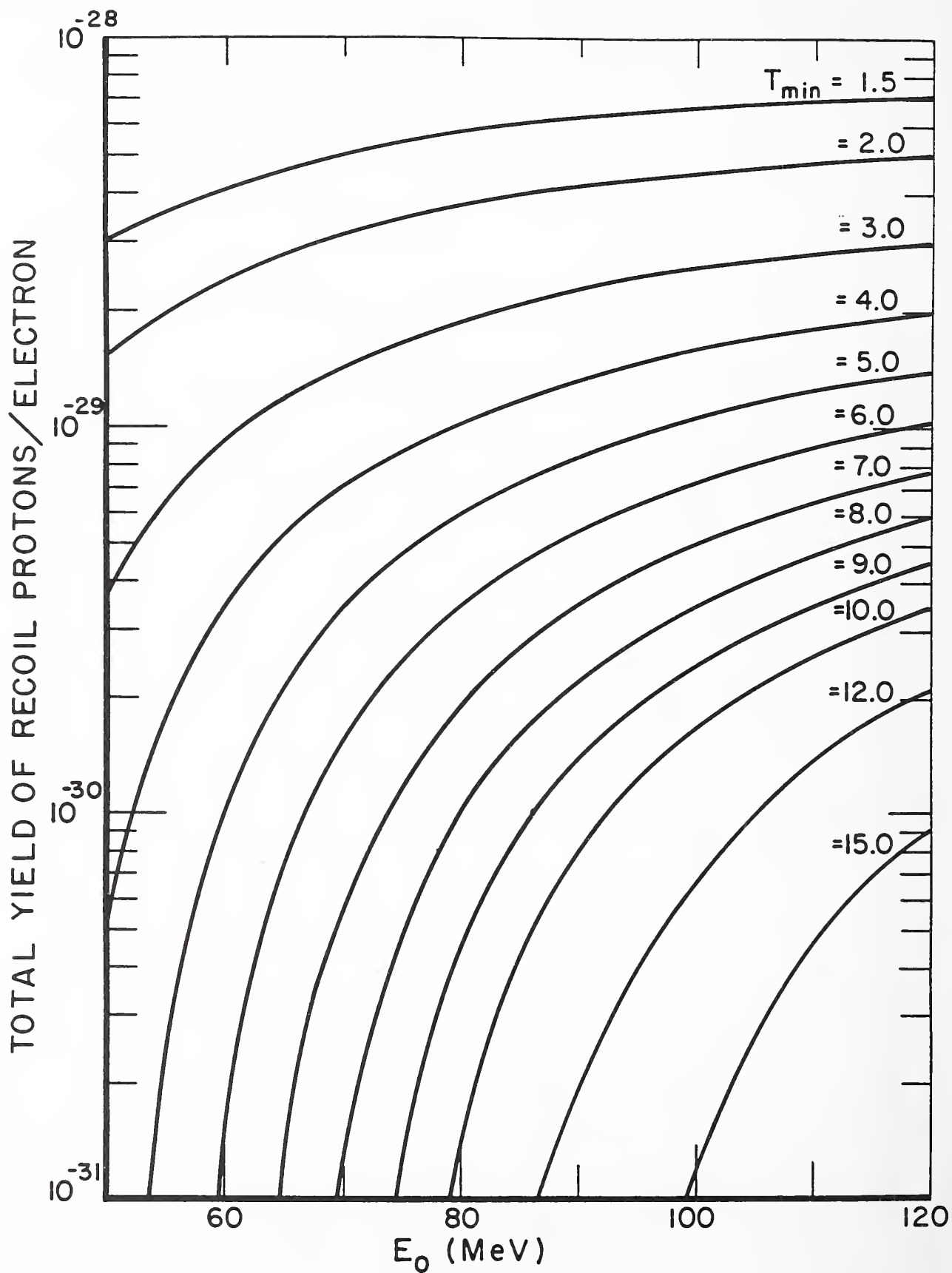


Fig. 21



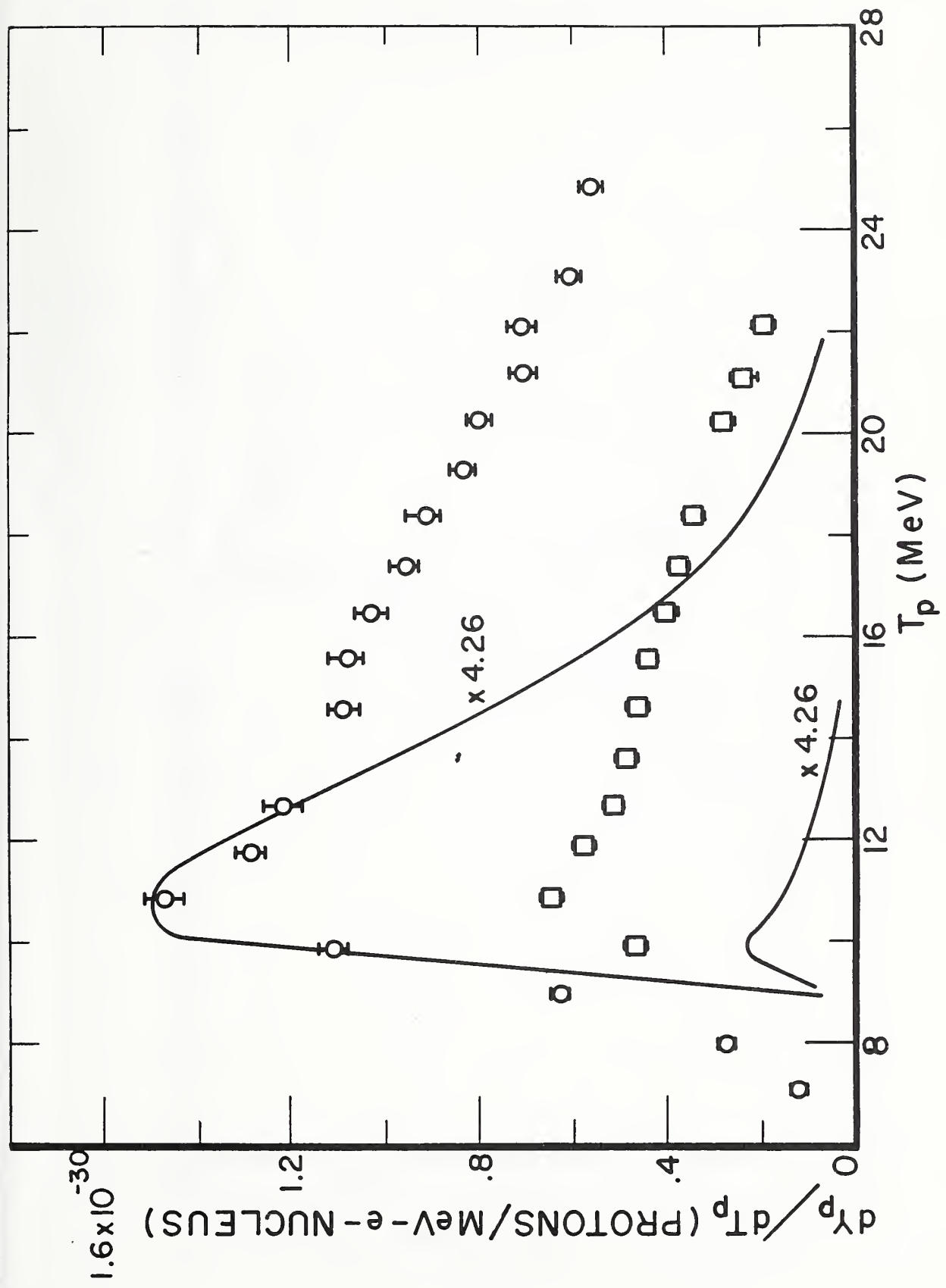
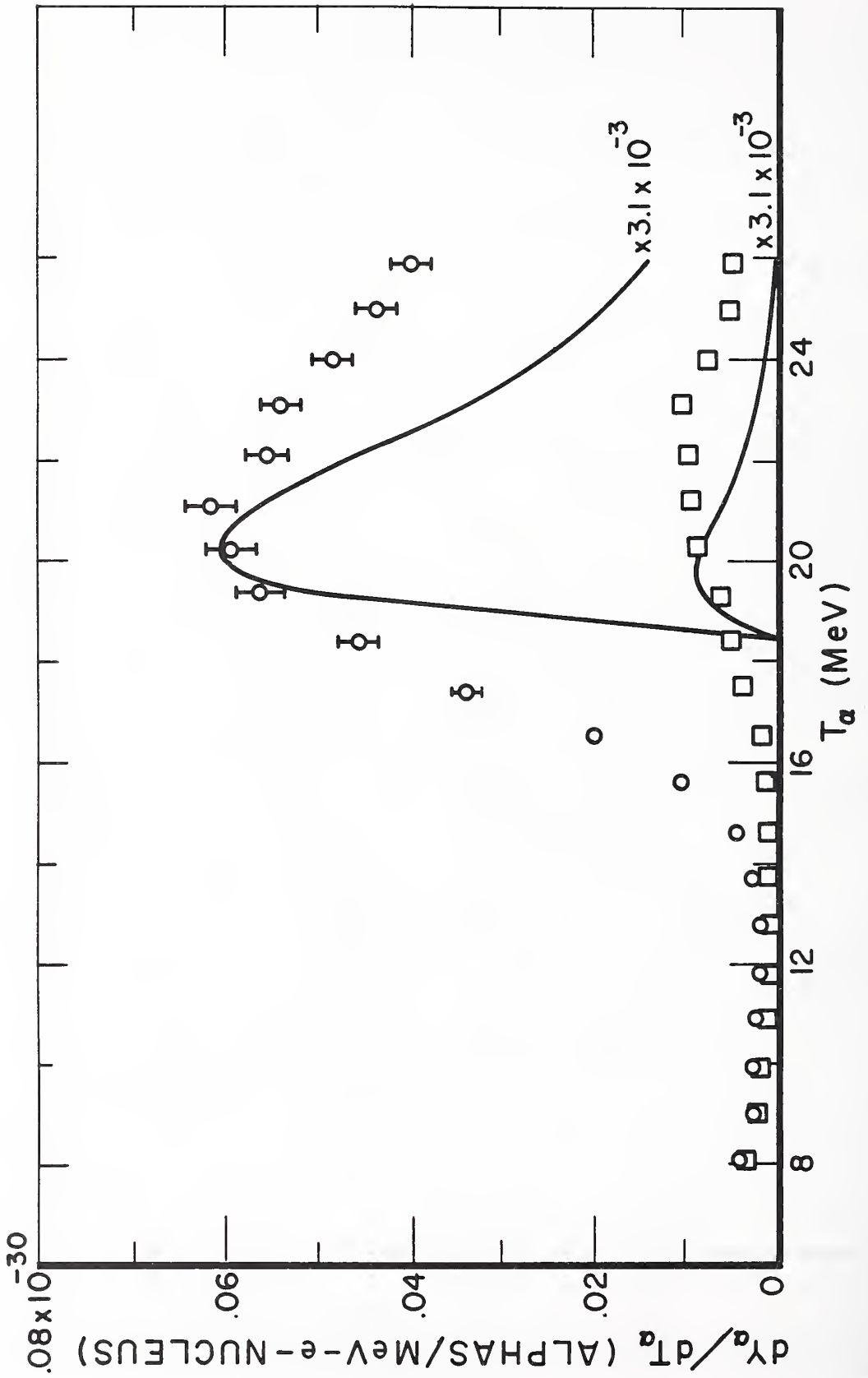


FIG. 23



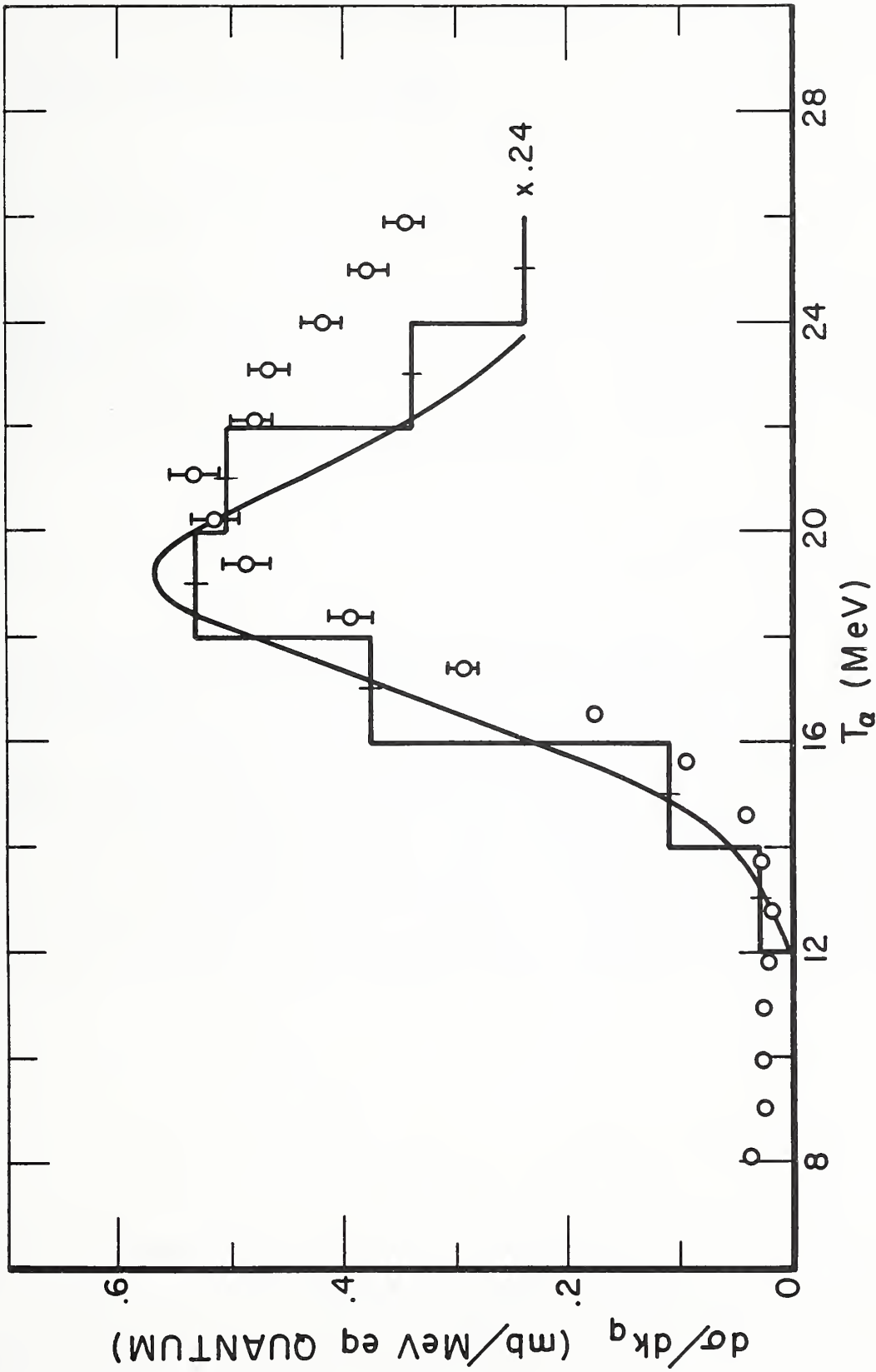


FIG. 25



1. PUBLICATION OR REPORT NUMBER NISTIR 4495
2. PERFORMING ORGANIZATION REPORT NUMBER
3. PUBLICATION DATE JUNE 1991

BIBLIOGRAPHIC DATA SHEET

7. TITLE AND SUBTITLE
 Evidence for surface α particle clusters in ^{nat}Ag and ^{197}Au from the (e,α) reaction

8. AUTHOR(S)
 R. Dodge

9. PERFORMING ORGANIZATION (IF JOINT OR OTHER THAN NIST, SEE INSTRUCTIONS)
 DEPARTMENT OF COMMERCE
 NATIONAL INSTITUTE OF STANDARDS AND TECHNOLOGY
 GAITHERSBURG, MD 20899

7. CONTRACT/GRANT NUMBER
8. TYPE OF REPORT AND PERIOD COVERED

10. PERFORMING ORGANIZATION NAME AND COMPLETE ADDRESS (STREET, CITY, STATE, ZIP)

11. SUPPLEMENTARY NOTES

12. DOCUMENT DESCRIBES A COMPUTER PROGRAM; SF-185, FIPS SOFTWARE SUMMARY, IS ATTACHED.

13. ABSTRACT (A 200-WORD OR LESS FACTUAL SUMMARY OF MOST SIGNIFICANT INFORMATION. IF DOCUMENT INCLUDES A SIGNIFICANT BIBLIOGRAPHY OR LITERATURE SURVEY, MENTION IT HERE.)

The ^{nat}Ag and ^{197}Au (e,p) and (e,α) energy and angular distributions were measured at 6 electron bombarding energies between 50 and 115 MeV at the National Institute of Standards and Technology. The ^{nat}Ag and ^{197}Au (e,p) angular distributions exhibit an asymmetric component which increases from 0 to 50% as the proton energy increases from the proton Coulomb barrier to 26 MeV. The ^{nat}Ag and ^{197}Au (e,α) angular distributions exhibit an asymmetric component which increases from 0 to 30% as the α energy increases from the α particle Coulomb barrier to 26 MeV. We conclude that the asymmetric component of the proton and α particle yields are the result of direct or semidirect processes rather than resonance processes and hence, because of the short mean free paths of α particles in nuclear matter, give evidence for the existence of α particle clusters in the nuclear surface.

14. KEY WORDS (6 TO 12 ENTRIES; ALPHABETICAL ORDER; CAPITALIZE ONLY PROPER NAMES; AND SEPARATE KEY WORDS BY SEMICOLONS)

alpha particle clusters; alpha particle yields; angular distributions; electronuclear physics; electroproduction of alphas; electroproduction of protons; energy distributions; gold 197; nuclear surface; proton yields; silver

15. AVAILABILITY
 UNLIMITED
 FOR OFFICIAL DISTRIBUTION. DO NOT RELEASE TO NATIONAL TECHNICAL INFORMATION SERVICE (NTIS).
 ORDER FROM SUPERINTENDENT OF DOCUMENTS, U.S. GOVERNMENT PRINTING OFFICE, WASHINGTON, DC 20402.
 ORDER FROM NATIONAL TECHNICAL INFORMATION SERVICE (NTIS), SPRINGFIELD, VA 22161.

14. NUMBER OF PRINTED PAGES 56
15. PRICE A04





